Progress in Oceanography 219 (2023) 103125

Contents lists available at ScienceDirect

Progress in Oceanography

journal homepage: www.elsevier.com/locate/pocean

Seasonal dynamics of phytoplankton community assembly at the Blanes Bay Microbial Observatory (BBMO), NW Mediterranean Sea

Sergio M. Vallina [a,*,1], Charlie Gaborit [b,*,1], Celia Marrase [b], Josep M. Gasol [b], Nixon Bahamon [b,c], Michael J. Follows [d], Guillaume Le Gland [b], Pedro Cermeño [b]

[a] Gijón Oceanography Centre (CSIC), Ave Príncipe de Asturias 70 Bis, 33212 Gijón, Asturias, Spain
[b] Institute of Marine Sciences (CSIC), Passeig Marítim de la Barceloneta 37, 08003 Barcelona, Catalonia, Spain
[c] Blanes Centre for Advanced Studies (CSIC), Carrer Accés Cala Sant Francesc 14, 17300 Blanes, Catalonia, Spain
[d] Department of Earth, Atmospheric and Planetary Sciences (MIT), 77 Massachusetts Ave, Cambridge, MA 02139, USA

ARTICLE INFO

Keywords:
Seasonal dynamics
Phytoplankton community assembly
Environmental factors
Climatic year
Ecological niches
Niche *vs* neutral theory
Mechanistic modeling

ABSTRACT

The dynamics of phytoplankton biomass and community composition is important for the functioning of marine ecosystems and ocean biogeochemical cycles. However, there is a shortage of studies addressing the interannual seasonal patterns of phytoplankton community assembly due to sampling limitations. Here we study the seasonal dynamics of eight major phytoplankton groups over a 12 year period (2006 to 2018) using a time-series of taxonomic composition from the Blanes Bay Microbial Observatory (BBMO) in the North Western Mediterranean Sea: dinoflagellates, diatoms, coccolithophores, *Prochlorococcus*, *Synechococcus*, picoeukaryotes, nanoeukaryotes, and photosynthetic nanoflagellates. We combine the analysis of biotic factors (primary production, phytoplankton taxa, cell abundance, cell size, chlorophyll-a concentration, and phytoplankton biomass) and abiotic factors (nutrients, temperature, and irradiance) to provide a coherent picture of the observed seasonal patterns of phytoplankton community assembly. The BBMO ecosystem is seasonally heterogeneous in community composition, displaying large fluctuating alternations in phytoplankton group dominance throughout the year. The seasonal succession of phytoplankton groups tends to repeat itself every year in a regular fashion, being the seasonal variability of the phytoplankton groups larger than their interannual variability. We compute α-diversity, a measure of the *effective richness* of phytoplankton groups. The seasonality of α-diversity shows that it is lowest during winter and highest during summer. We compute temporal β-diversity, a measure of compositional heterogeneity of the phytoplankton community. The data show a sinusoidal behavior of β-diversity as a function of the temporal distance between samples, with a period of one year. We use the mirror index (1 - β-diversity) at a temporal distance of one month to compute the phytoplankton group turnover. The seasonality of turnover shows that it is highest during spring and autumn. To evaluate the validity of niche and neutral theories in predicting the interannual sinusoidal behavior of β-diversity, we performed numerical simulations using a mechanistic model. The results provide support to the niche theory for marine phytoplankton ecology and community assembly. The phytoplankton groups appear to follow their specific ecological niches, tracking the seasonal changes in environmental conditions. The ecological implications of these findings are that marine phytoplankton groups appear to fill distinct environmental niches and thus may have different functional roles in the ecosystem. Furthermore, they may be predictable using both mechanistic and species distribution modeling approaches. The climatological time-series presented here can be an excellent testing ground for evaluating the performance of these marine ecosystem models having an explicit representation of different phytoplankton groups.

1. Introduction

Marine phytoplankton are responsible for about half of the net annual primary production on Earth (Field et al., 1998), sustaining marine food webs and productive fisheries, and contributing to the draw-down of atmospheric CO2 through the export of organic carbon into the deep ocean by affecting some the several biological carbon pumps (Claustre et al., 2021). Phytoplankton are a highly diverse polyphyletic group composed of several prokaryotic cyanobacteria and

* Corresponding authors.
E-mail addresses: sergio.vallina@csic.es (S.M. Vallina), gaborit@icm.csic.es (C. Gaborit).
[1] These authors contributed equally to this work. https://orcid.org/0000-0002-1335-9237.

https://doi.org/10.1016/j.pocean.2023.103125
Received 9 October 2022; Received in revised form 29 July 2023; Accepted 19 September 2023
Available online 4 October 2023

eukaryotic microalgae (protists) that exhibit a large range of sizes (from less than 1 μm to more than 100 μm in equivalent spherical diameter), shapes, and ecological interactions (Finkel et al., 2010). Some phytoplankton groups can also serve as biological indicators for ecosystem functioning and health status (Racault et al., 2014).

The seasonal succession and biogeography of phytoplankton groups in the Mediterranean Sea has been the focus of study for several decades (Ribera-D'alcala et al., 2004; Charles et al., 2005; D'Ortenzio and d'Alcala, 2009; Siokou-Frangou et al., 2010). The frequency and intensity of environmental events (i.e. wind speed, freshening events) (Bernardello et al., 2012) combined to phytoplankton species traits has been observed to affect phytoplankton blooms and community composition (Aubry et al., 2004; Ribera-D'alcala et al., 2004). Both food web interactions and environmental factors have been reported as drivers of changes in phytoplankton biomass and community composition, and therefore the temporal variability of environmental conditions can lead to a seasonal succession of phytoplankton groups (Margalef, 1974). In coastal areas of north-western (NW) Mediterranean Sea like the Blanes Bay, the biogeochemical water properties are strongly dependent on the input of nutrients to the surface waters due to riverine discharges and vertical upwelling by turbulent mixing (Charles et al., 2005; Guadayol et al., 2009). Over the shallow inshore waters (<50 m depth) mesoscale circulation plays an important role in shelf-slope exchange, conferring the inshore waters with similar biogeochemical conditions than those prevailing offshore (Estrada et al., 2014; Ahumada-Sempoal et al., 2015; Bahamon et al., 2020). The BBMO station thus behaves similarly to the offshore station located in the Blanes canyon, which has a much deeper water column (>200 m). In particular, there is a pronounced late-winter or early-spring phytoplankton bloom with the highest primary production after the deepening of the mixed layer, which brings nutrient-rich deep waters into the surface and over the shelf (Nunes et al., 2018).

Ecological niches refer to the environmental conditions (e.g. nutrient concentration, water temperature, solar irradiance, etc.) where organisms can grow and compete with other organisms (Irwin et al., 2012). The *niche theory* states that some plankton species or ecotypes will dominate in some ecological niches but not in others due to differences in their physiological traits, which translate into differential competitive ability among ecotypes depending on the environmental niche where they are located (MacArthur, 1968). Niche theory is the cornerstone of current trait-based modeling approaches (Litchman and Klausmeier, 2008), either using numerical (mechanistic) models (Follows and Dutkiewicz, 2011) or using spatial-distribution (statistical) models (Righetti et al., 2019). However, the rules of community assembly are still object of conceptual debate, being *neutral theory* an alternative candidate to explain it (Hubbell, 2001). Neutral theory states that different species or ecotypes are ecologically equivalent and that niche differences do not influence their competitive ability (i.e. resource competition is neutral) and their biomass. That is, all species have the same probability of being found in any niche because they have the same competitive ability (ecological fitness) (Weistuch et al., 2022). The fact that the local community composition has only a subset of the regional pool of species, and that their relative biomass are not evenly distributed, is explained by dispersal limitation and stochastic demographic processes (Villarino et al., 2018). In other words, under neutral theory dynamics, the local community assembly is the result of random immigration/emigration processes by means of dispersal and random demographic processes (Hubbell, 2001, 2005). The relative biomass of species (their percentage of total biomass) is assumed not to be affected by environmental conditions such as nutrient concentration, temperature, solar radiation. This is in stark contrast to niche theory, that assumes that relative biomass of species is strongly affected by environmental conditions. Niche theory and neutral theory are thought of being two opposing theories to explain the processes underlying the assembly of communities. Furthermore, even if they are in open conflict with each other on theoretical grounds, both theories have been applied successfully to explain marine plankton community assembly (e.g. see Cadotte (2017), Wootton (2005), Irwin et al. (2015) and Follows et al. (2007) for niche theory and see Chust et al. (2012) and Villarino et al. (2018) for neutral theory). However, there is a shortage of observational studies addressing the validity of either theory when applied to time-series of marine phytoplankton. Therefore, the question of which theory explains better the observed patterns is still open and this article aims at help resolving the controversy using long-term observational data.

Here we analyze 12 years of environmental variables and phytoplankton community composition at the Blanes Bay Marine Observatory (http://bbmo.icm.csic.es) with the aim of reconstructing the architecture of ecological niches that determine the seasonal succession of phytoplankton in this temperate coastal ecosystem. We analyze for each phytoplankton group the combination of environmental variables that best determine their seasonal distribution and quantify the recurrence of taxa and groups throughout the 12-year time series in order to determine to what extent these patterns are influenced by interannual variability in climatic/oceanographic variability and/or anthropogenic impacts. Ocean plankton ecosystem models suffer from the lack of robust and detailed time series against which to compare the results of their predictions. The results of the present study provide an unprecedented analysis of niche preferences by the different phytoplankton groups throughout 12 annual cycles, offering an excellent dataset for validating ocean plankton ecosystem models. By constructing a climatic year with all observed variables, we show that different phytoplankton groups follow distinct ecological niches and thus respond differently (and asynchronously) to seasonal changes in environmental conditions. Furthermore, we find a seasonal cycle in the relative biomass of species and phytoplankton groups (i.e. a sinusoidal behavior of the interannual β-diversity), which supports niche-dynamics.

2. Materials and methods

2.1. Research location

The Blanes Bay Microbial observatory (BBMO) or station 1 is located in the north-west Mediterranean Sea as part of the Catalan coast. The BBMO is found 70 km north from Barcelona (Spain), approximately 1 km offshore (41°67N, 2°79E). The operational observatory of the catalan sea (OOCS) or station 2 is found on the Blanes Canyon, and therefore it is further offshore (41°66N, 2°90E) (see Fig. 1). These two observatories provide different but complementary datasets (Bahamon et al., 2011). The BBMO sampling point (station 1) has a maximum depth of ≈20 m and it is located between the submarine Blanes Canyon to the north and La Tordera River to the south (for an inset image of the Blanes Bay area see Figure 1 in Guadayol et al. (2009)). River discharge volume has been shown to follow the dynamics of precipitation, although a seasonal pattern could not be established (Guadayol et al., 2009). The sampling at BBMO was done monthly at the surface layer (0–5 m depth). The sampling period covers 12 years from mid June 2006 until March 2018, with some months (5 out of 142) occasionally being missed due to logistic reasons. These missing values were filled using a gap-filling approach that consists on first imposing their climatological value and then passing a temporal runmean smoothing. Please note that the gap-filled values were not used for the statistical analyses. The OOCS sampling point (station 2) has a maximum depth of ≈200 m and it is located on the submarine Blanes Canyon. The sampling at OOCS was done monthly for the whole column-water (0–200 m depth). The sampling period covers 9 years from March 2009 to March 2018. Note that the microbial variables were only measured at BBMO sampling point (station 1); therefore, we do not have a depth-resolved view of the phytoplankton species composition or primary production, only surface time-series at Blanes Bay.

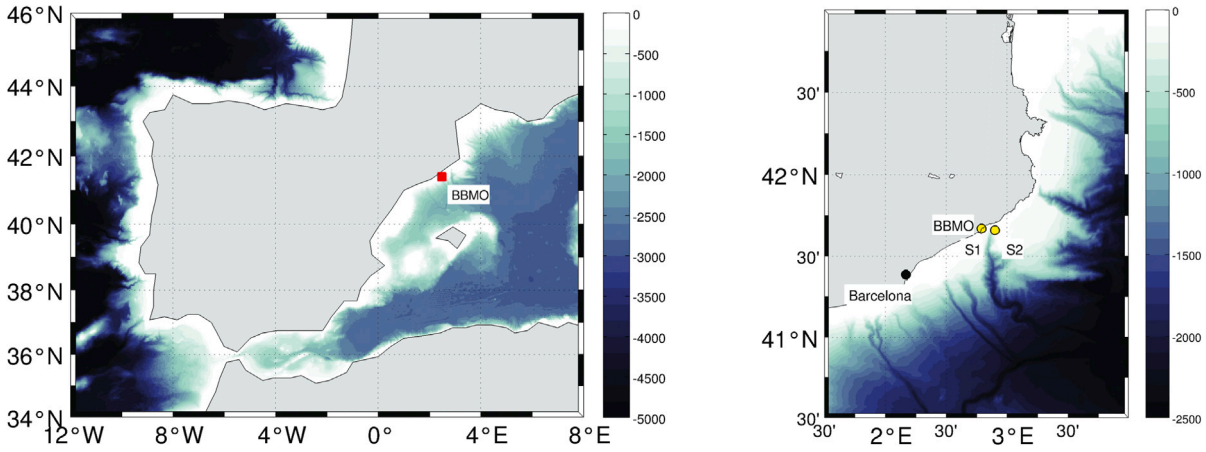

Fig. 1. Location of the Blanes Bay Microbial observatory (BBMO) and location of the Operational Observatory of the Catalan Sea (OOCS), both in the north-west Mediterranean Sea. The BBMO station (1) is found 70 km north from Barcelona (Spain), approximately 1 km offshore (41°67N, 2°79E). The OOCS station (2) is found on the Blanes Canyon, and therefore it is further offshore (41°66N, 2°90E).

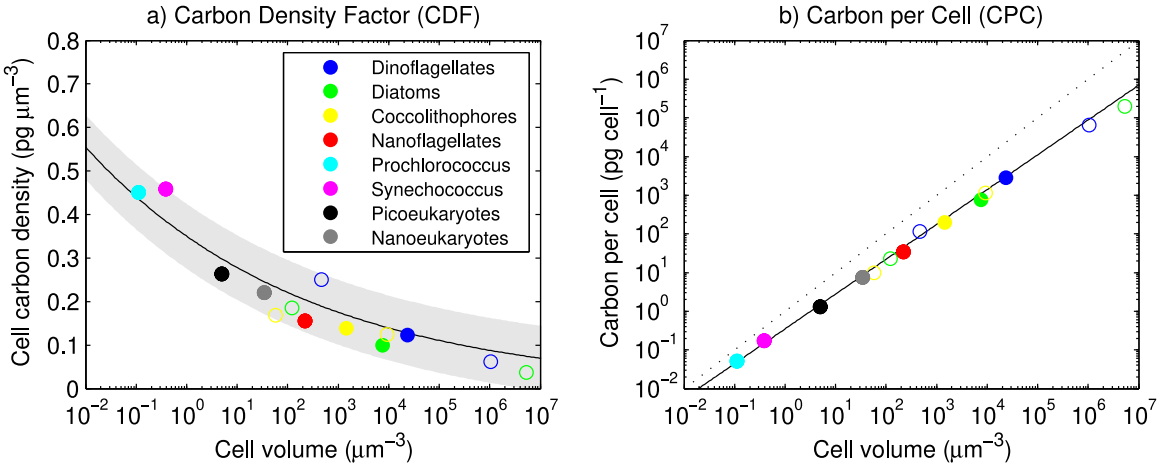

Fig. 2. Allometric carbon density factor (CDF) as function of cell volume computed using the biomass-weighted (geometric) mean of the equivalent spherical diameter (ESD) for each phytoplankton group (left panel) and the corresponding carbon per cell (CPC) for each phytoplankton group (right panel). The colored dots are alternative CDF and CPC estimates derived from the literature using different allometries for each phytoplankton group (see Methods for details). The colored open circles are the corresponding CDF and CDF for the smallest and largest ESD value within each phytoplankton group. The CDF decreases five-fold from a cell size of ESD = 0.5 µm to a cell size of ESD = 64 µm, which is a size range that encompasses the lower and upper limits of the mean ESD for all phytoplankton groups. The carbon per cell (pgC cell^{-1}) increases linearly with cell volume clearly below the isometric size-scaling due to the negative allometry of carbon density (pgC um^{-3}) with cell volume. Note that 0.1 (pgC um^{-3}) = 0.1 (gC cm^{-3}) = 100.0 (kgC m^{-3}).

2.2. Phytoplankton variables

A total of 162 water samples of one hundred milliliters (100 ml) were collected. The samples were preserved with buffered formaldehyde/hexamine reagent, and were kept in a dark cold room (4 °C) until analysis. In the lab, the samples were subject to cell counting and taxonomic assignment under inverted microscope (XSB-1 A), following the Utermöhl (1958) method. Cell density is expressed in number of cells per liter. Flow cytometry was used to identify and count *Synechococcus*, *Prochlorococcus*, picoeukaryotes, nanoeukaryotes, and photosynthetic nanoflagellates (or PNF) by means of epifluorescence. All observed species were thus classified as belonging to one of the eight major phytoplankton groups observed in the study site: dinoflagellates, diatoms, coccolithophores, *Prochlorococcus*, *Synechococcus*, picoeukaryotes, nanoeukaryotes, and photosynthetic nanoflagellates. Any dinoflagellate species without chla content was discarded to exclude the *obligate predatory* species from the analysis, only photosynthetic dinoflagellate were kept in the list; however, there is still potential for *facultative predatory* mixotrophy among them. The three phytoplankton groups for which the taxonomic composition is resolved to the level of species are: dinoflagellates, diatoms, and coccolithophores. For the other five groups, their cell sizes are too small to be classified to the species level using microscopical approaches. The cell size (as equivalent spherical diameter or ESD) was converted to cell volume using the diameter of each species of phytoplankton. The biovolume of each species was then computed as the number of cells times their volume. The conversion from biovolume to biomass was done using an allometric carbon density factor (pgC µm^{-3}) $\mathrm{CDF} = \alpha\, \mathrm{V}^{\beta}$, where $\alpha = 0.35$ and $\beta = -0.10$ (see Fig. 2a). This allometry simplifies the conversion to biomass by merging into a single power-law the several allometries described for each phytoplankton group independently (Verity et al., 1992; Menden-Deuer and Lessard, 2000; Montagnes and Franklin, 2001; DuRand et al., 2002; Segura-Noguera et al., 2012; Simó et al., 2009; Guadayol et al., 2009; Graff et al., 2012), with minor deviations from the predicted carbon per cell or CPC (pgC cell^{-1}) when using different allometries for each group (see Fig. 2b). The allometric carbon density factor was applied to the biovolume of each species (i.e. cell volume times their abundance) in order to estimate the carbon biomass of each species per sample. Using an allometric CDF is most appropriate than a constant conversion because small cells usually contain more carbon per unit volume than large cells (Verity et al., 1992). Please note that the ESD (and thus the

volume) of the counted cells by optical microscopy or flow cytometry was not measured directly and a constant ESD was used instead for each species based on literature values.

2.3. CHEMTAX analysis

The CHEMTAX computer program (Latasa, 2007) was used to compute the relative contribution of different phytoplankton groups to total chla, based on a series of marker pigments (Nunes et al., 2018). CHEMTAX uses an initial matrix of pigment-to-chla ratios for all the phytoplankton groups under study and seeks to optimize the pigment-to-chla ratios of the matrix to generate an estimate of the contribution of each group to total chla. Before running CHEMTAX, the samples were clustered according to the contribution of their specific pigments (Nunes et al., 2018). The similarity matrix among samples was computed using Manhattan or Hamming distances (i.e. rectilinear L_1 distances); then the samples were clustered using the Minimum variance method (Ward, 1963; Legendre and Legendre, 1998). Following the procedure described by Latasa (2007) and Latasa et al. (2010), a set of 29 random initial pigment-ratio matrices were created considering eight phytoplankton pigment groups: cryptophytes, diatoms, dinoflagellates, haptophytes (e.g. Chrysochromulina, Phaeocystis, Emiliana huxleyi), pelagophytes, prasinophytes, *Prochlorococcus* and *Synechococcus*. We assumed that chlorophytes in Blanes Bay were basically represented by prasinophytes (Nunes et al., 2018). Eight successive CHEMTAX runs were performed with the 29 matrices. A single average pigment-ratio matrix was obtained from the eighth run of the 29 matrices. This average matrix was run again to estimate the contribution of each phytoplankton pigment group to the total chla in the sample. This procedure was performed independently with each cluster of samples (see Nunes et al. (2018) for details).

2.4. Environmental variables

Nutrients (nitrate, ammonium, phosphate, silicate) were measured colorimetrically with an autoanalyser following Hansen and Koroleff's method (Hansen and Koroleff, 1999). Here we will show the time-series of nitrate (NO3), ammonium (NH4), and silicate; but dissolved inorganic phosphorous (not shown) correlates well with dissolved inorganic nitrogen (DIN = NO3 + NH4). Note that although nitrate, ammonium, silicate are ions or cations, we have removed the electrical charge (negative or positive) from their acronym for the sake of simplicity. Temperature, conductivity and depth were measured using a multi-parametric probe (CTD). Ancillary sensors in the CTD allowed measuring photosynthetic active radiation (PAR). Chlorophyll-a (chla) concentration was measured by fluorometry (Turner Designs fluorometer) in 6.5 ml extracts (90% acetone, 4 C, overnight) of 150 ml of seawater filtered through GF/F (Whatman) (Gasol et al., 2016).

2.5. Climatological averaging

The time-series of all variables were binned on a monthly grid and then mean values were computed for each month. The monthly means were used to build a standard climatological year. We also performed a smoothing *harmonics regression* (Bloomfield, 2000; Chatfield, 2004) to fit the climatological data using sinusoidal functions at two frequencies ω_j: (1) one cycle per year (twelve-month periodicity) and (2) two cycles per year (six-month periodicity). Harmonics regression is based on the fact that any periodic signal (e.g. our climatologies) can be approximated by the sum of sinusoidal (sine and cosine) functions (see Box 1). The time-series $y(t)$ is a periodic signal of period$T$ = 1 year, and the angular frequency (ω_j) of its jth harmonic is equal to (j/T). The fit to this periodic data can be done using linear regression to obtain the parameters α_j and β_j of the linear Eq. (1) (see Box 1). With α_j and β_j computed, we can then obtain the wave amplitudes A_j and temporal phases θ_j of each harmonic function (see Box 1). Particularly the amplitude of each harmonic is important because it provides information of the importance or relative contribution of its frequency to the signal being fitted. We will show that the annual frequency (1st harmonic) clearly dominates all the y(t) climatological signals that we have evaluated at BBMO. The climatology for PAR was constructed using astronomical functions because the in-situ measurements were extremely noisy due to the low frequency of sampling and stochastic cloud coverage. The daily averaged solar irradiance at the top-of-the-atmosphere was first calculated following Stull (2000) and Brock (1981) and then converted into ocean-surface irradiance considering a transmission coefficient of 0.5; that is, an atmospheric reduction by a half (Kiehl and Trenberth, 1997). PAR was then finally obtained assuming that only 50% of total surface irradiance belongs to the PAR wavelengths. All the analyses were performed using **GNU Octave** scientific programming language (free open-source software https://octave.org/).

2.6. Primary production

Primary production (mmolC m^{-3} day^{-1}) was measured *directly* in the lab using the 14C method (Steeman-Nielsen, 1952) from photosynthesis–irradiance (P-E) curves. The methodology is described in detail by Gasol et al. (2016). Another estimate of primary production was computed *indirectly* combining a diagnostic modeling approach with chla observations. The alternative chla-based estimate of phytoplankton biomass is used to cross-validate the phytoplankton biomass estimate from microscopic cell counts. The alternative modeling-based estimate of primary production is validated with the direct measurements and was used to estimate the fraction of regenerated production driven by ammonium uptake (i.e. one minus the f_{ratio}) (Eppley and Peterson, 1979). The approach is conceptually straightforward: chlorophyll-a measurements are converted to total phytoplankton biomass by means of a carbon-to-chla ratio that is a function of irradiance levels following Lefevre et al. (2002) and Vallina (2008b) (see Eqs. (18), (19)). Concentration values of nitrate and ammonium are used to compute the nutrient limitation of primary production assuming Michaelis–Menten uptake curves, with a preferential uptake of ammonium (Vallina and Le Quéré, 2008) (see Eqs. (16), (17)). This nutrient limitation vary between 0 (no growth) and 1 (unlimited growth). We decided to use a nitrogen-based model (instead of a phosphorous-based model) in order to distinguish between new and regenerated production. Nevertheless, total DIN and PO4 are well correlated (not shown). The irradiance limitation is computed following Cropp et al. (2004) by assuming a decrease in light limitation up until a saturating level, after which there is photo-inhibition (see Eq. (15)). Temperature limitation is accounted for by means of canonical Q_{10} function (see Eq. (14)). Primary production on nitrate (N) and on ammonium (A) was then estimated independently after multiplying the biomass-specific uptake rates for these nutrient types (see Eqs. (12), (13)) by the phytoplankton biomass estimated from the chla concentration (see Eqs. (10), (11)). Finally, the fraction of primary production due to ammonium uptake (1 - f_{ratio}) can be computed by dividing regenerated production over total primary production (see Eqs. (8), (9)). Box 2 provides the equations and Table 1 the model parameters used to compute this alternative estimate of primary production.

Box 1 | Harmonics regression

$$y(t) = \sum A_j \, sin(x_j + \theta_j)$$
$$= \sum A_j \, sin(x_j) \, cos(\theta_j) + \sum A_j \, cos(x_j) \, sin(\theta_j)$$
$$= \sum A_j \, sin(x_j) \, (\alpha_j / A_j) + \sum A_j \, cos(x_j) \, (\beta_j / A_j)$$
$$= \sum \alpha_j \, sin(x_j) + \sum \beta_j \, cos(x_j) \quad (1)$$

$$x_j(t) = (2\,\pi\,\omega_j)\,t \quad (2)$$

$$\alpha_j = A_j \, cos(\theta_j) \quad (3)$$

$$\beta_j = A_j \, sin(\theta_j) \quad (4)$$

$$A_j = \sqrt{\alpha_j^2 + \beta_j^2} \quad (5)$$

$$\theta_j = \quad acos(\alpha_j / A_j) \quad if \quad \beta_j \geq 0 \quad (6)$$

$$\theta_j = 2\,\pi - acos(\alpha_j / A_j) \quad if \quad \beta_j < 0 \quad (7)$$

Box 2 | Regenerated production fraction

- Primary Production (mmolC m^{-3} day^{-1}) and fraction of regenerated production (n.d.)

$$PP = PP_N + PP_A \quad (8)$$

$$(1 - f_{ratio}) = \frac{PP_A}{PP} \quad (9)$$

- New production (on nitrate) and regenerated production (on ammonium)

$$PP_N = \mu_N \, Phy \quad (10)$$

$$PP_A = \mu_A \, Phy \quad (11)$$

- Biomass-specific nutrient uptake rates (day^{-1}) on nitrate (N) and on ammonium (A)

$$\mu_N = (\gamma_N \, \gamma_T \, \gamma_I) \, \mu_{max} \quad (12)$$

$$\mu_A = (\gamma_A \, \gamma_T \, \gamma_I) \, \mu_{max} \quad (13)$$

- Environmental limitation (n.d.) due to temperature, irradiance, nitrate, ammonium

$$\gamma_T = Q_{10}^{(T - T_{max})/10} \quad (14)$$

$$\gamma_I = \frac{I}{I_{sat}} \exp\left(1 - \frac{I}{I_{sat}}\right) \quad (15)$$

$$\gamma_N = \frac{N}{K_N + N} \left(1 - \gamma_A\right) \quad (16)$$

$$\gamma_A = \frac{A}{K_A + A} \quad (17)$$

- Phytoplankton biomass (mmolC m^{-3}) and carbon-to-chla ratio (mgC $mgChla^{-1}$)

$$Phy = (Q_{C:Chla} / 12.0) \, Chla \quad (18)$$

$$Q_{C:Chla} = Q_{max} - (Q_{max} - Q_{min}) \, \frac{(I_{max} - I)}{(I_{max} - I_{min})} \quad (19)$$

2.7. Growth rate

Neither the primary production $Fphy$ (mmolC m^{-3} d^{-1}) nor the biomass-specific growth rate μ (d^{-1}) of each phytoplankton group were directly measured at BBMO. However, we can tentatively provide a back-of-the-envelope estimate using the following approach:

$$\frac{d\,Phy(i)}{dt} = Fphy(i) - Lphy(i) \quad (20)$$

$$Fphy(i) = \phi(i) \;\; PP_{tot} \quad (21)$$

$$\phi(i) = Phy(i)^n / \sum Phy(i)^n \quad (22)$$

$$n = 2.0$$

The left-hand side of Eq. (20) is the time-derivative ($\frac{d\,Phy}{dt}$) computed on the smooth climatological time-series (e.g. harmonics fit to the data) for the biomass of phytoplankton group i. The right-hand side of Eq. (20) is the balance between total gains by primary production (growth) and total losses by all mechanisms (grazing, mortality, sinking, advection, etc.). The first term on the right-hand side of Eq. (20) is the time-series of primary production $Fphy$ (mmolC m^{-3} d^{-1}) for each phytoplankton group i that we would like to estimate using some assumptions. In particular, we assume that the primary production of each phytoplankton group i equals the measured (14C) total primary production, times a metric of their relative contribution ϕ (n.d.). The relative contribution is assumed to be non-linear (quadratic): the squared biomass of phytoplankton group i is divided by the sum of the squared biomass of all other groups. This is implicitly assuming that the biomass-specific growth rate (d^{-1}) of phytoplankton group i is highest when it peaks seasonally or even dominates the community and lower when it does not. The rationale is that in order to dominate the community locally, the group i must be growing faster per-capita than the others. Once the primary production for each group has been estimated, we can then compute the time-series of their biomass-specific growth rate $\mu = Fphy/Phy$ (d^{-1}). Likewise, the second term on the right-hand side of Eq. (20) can be computed algebraically $Lphy = Fphy - \frac{d\,Phy}{dt}$ (mmolC m^{-3} d^{-1}).

2.8. β-Diversity

We use the Bray–Curtis similarity index as our β-diversity estimator, a measure of compositional similarity (Faith et al., 1987) of the phytoplankton community that can be understood as species turnover when computed in time. The Bray–Curtis similarity is a biomass-weighted index of community similarity. That is, both the community composition and the biomass of the phytoplankton species (or phytoplankton groups) present in the community are taken into account. To avoid any bias due to seasonal changes in total phytoplankton biomass, when computing the temporal β-diversity with Bray–Curtis similarity, one should use relative values of biomass (i.e. the relative contribution or proportion of each species to total biomass) as weights, instead of absolute values of biomass (Legendre and Legendre, 1998). When each sample is a vector with the relative proportions to the total community of the species it contains, the Bray–Curtis *dissimilarity* is equivalent to the Manhattan or Hamming distance (i.e. rectilinear L_1 distance), times a normalization factor of one half (Kaufman and Rousseeuw, 1990; Legendre and Legendre, 1998). The Bray–Curtis similarity is computed pair-wise between all samples. Therefore, we can plot β-diversity as a function of temporal distance between samples (i.e. the time-lag between them). The neutral theory predicts an absence of relationship between relative biomass and environmental conditions (nutrients, temperature and light), and thus predicts an absence of seasonal cycle in relative biomass. Under neutral theory, the Bray–Curtis distance as a function of time-lag should have a maximum at the start (time-lag = 0) and then decay towards a white noise signal. That is, neutral theory predicts an exponential decay of community similarity with temporal distance, while niche theory predicts a sinusoidal pattern. To evaluate

Table 1
List of model parameters.

Parameter	Sym	Value	Units
Maximum uptake rate	μ_{max}	1.2	d^{-1}
Half-sat for NO3 uptake	K_N	1.00	mmolN m^{-3}
Half-sat for NH4 uptake	K_A	2.00	mmolN m^{-3}
Temperature dependence	Q_{10}	1.20	n.d.
Maximum temperature	T_{max}	25.0	Celsius
Minimum carbon-to-chla	Q_{min}	30.0	mg mg^{-1}
Maximum carbon-to-chla	Q_{max}	100.0	mg mg^{-1}
Minimum irradiance	I_{min}	1.0	W m^{-2}
Maximum irradiance	I_{max}	180.0	W m^{-2}
Irradiance saturation	I_{sat}	60.0	W m^{-2}

the validity of the theoretical predictions of both niche theory and neutral theory against the observed patterns at BBMO, we use a mechanistic NPZD multi-species ecosystem model that allows for an easy transition from simulating a niche-dynamics community to simulating a neutral-dynamics community (Vallina et al., 2017). The ecosystem model is a simplified version of the MIT Darwin model (Follows et al., 2007) using a chemostat-bioreactor setup (see Appendix for a detailed description of the model equations and parameter values).

3. Results

3.1. Carbon per cell

Fig. 2a shows the allometric carbon density factor (CDF) as a function of cell volume computed using the biomass-weighted (geometric) mean of the ESD for each phytoplankton group. Fig. 2b shows the corresponding carbon per cell (CPC). Hereafter and for the sake of simplicity we will use the term *mean ESD* instead of *biomass-weighted geometric mean ESD*. Larger cells are less carbon-dense than smaller cells. The CDF decreases with cell size from 0.5 to 0.1 pgC um^{-3} between an ESD increasing from 0.5 to 64 μm, which is the ESD range that encompasses the lower and upper limits of the mean cell size for all phytoplankton groups. In particular, we have the following mean ESD per phytoplankton group: dinoflagellates 40 μm, diatoms 30 μm, coccolithophores 13.5 μm, photosynthetic nanoflagellates 7.5 μm, *Prochlorococcus* 0.6 μm, *Synechococcus* 0.9 μm, picoeukaryotes 2.1 μm, nanoeukaryotes 4.0 μm. The carbon per cell (pgC $cell^{-1}$) increases linearly with cell volume in log–log scale (that is, increases following a power-law in absolute scale) below the isometric size-scaling due to the negative allometry of carbon density (pgC um^{-3}) with cell volume. Sub-isometric size-scaling has been reported for many phytoplankton species and groups (Verity et al., 1992; Menden-Deuer and Lessard, 2000; Montagnes and Franklin, 2001; DuRand et al., 2002; Segura-Noguera et al., 2012; Graff et al., 2012) (but see Malerba et al. (2018)). Our values of carbon per cell at BBMO for *Prochlorococcus* (0.051 pgC $cell^{-1}$) and *Synechococcus* (0.175 pgC $cell^{-1}$) are similar to the values previously used at BATS for *Prochlorococcus* (0.056 pgC $cell^{-1}$) and *Synechococcus* (0.112 pgC $cell^{-1}$). Our values of carbon per cell for dinoflagellates (2865 pgC $cell^{-1}$), diatoms (758 pgC $cell^{-1}$), coccolithophores (200 pgC $cell^{-1}$), photosynthetic nanoflagellates (34.5 pgC $cell^{-1}$), nanoeukaryotes (7.5 pgC $cell^{-1}$), and picoeukaryotes (1.3 pgC $cell^{-1}$) are similar to those used in previous studies at BBMO (Simó et al., 2009; Guadayol et al., 2009).

3.2. Seasonal variability

The seasonal dynamics of environmental factors and phytoplankton at Blanes Bay (station 1) are reflective of a temperate ecosystem due to the strong influence of offshore waters from the Blanes Canyon (station 2) (see Fig. 3). The water column at station 2 is well mixed during winter, temperature being vertically homogeneous with values between ≈12–14 °C (see Fig. 3d). When the water column stratifies during summer, there is a strong vertical gradient with temperature values between ≈20–24 °C at the surface (see Fig. 3d). The mixed layer depth (MLD) is shown on top of the sea temperature field, from which it was computed as the thermocline middle point (largest gradient). MLD is correlated to temperature, with shallower depth in summer (warmer temperature) and deeper depth in winter (colder temperature). The two sampling stations BBMO and OOCS (see Fig. 1) display similar values and seasonality of the variables that they are both measuring, such as nutrients, temperature, irradiance, and chla (see Figs. 3 and 4). We can only assume (infer) that this may also be the case for the variables that are only measured at BBMO, such as the taxonomic composition of the phytoplankton community and primary production (see Figs. 5, 6, 7, 8). The seasonality of dissolved inorganic nutrients (DIN) such as nitrate and silicate at the surface tends to be negatively correlated to the sea surface temperature (SST) because the (i) winter-time upwelling offshore (>200 m) resulting from strong vertical mixing brings up higher nitrate and silicate concentration from deep cold waters, which then reach the BBMO inshore (<50 m depth) by horizontal mesoscale circulation, and (ii) by summer-time when the waters are warmer, most of the upwelled nutrients have been already consumed by primary producers (see Fig. 3; see Figs. 6a and c). Yet, even during summer the depletion of nutrients is incomplete due to remineralization of organic nitrogen to ammonium by bacterial activity (see Fig. 6b). Nitrate and silicate were below 0.6 mmol m^{-3} in summer and above 1.5 mmol m^{-3} in summer (see Figs. 6a and 6c). Ammonium has rather weak or flat seasonality (see Fig. 6b). Nutrients are tightly coupled to the winter mixing event of high vertical turbulence offshore (station 2) that is brought inshore (station 1) by fast horizontal mesoscale circulation. Therefore, primary production during the winter-time maximum is mostly new production (i.e. sustained by NO3 supply); while primary production during the summer-time minimum is mostly regenerated production (i.e. sustained by NH4 supply) (see Fig. 6i). We explain how to compute the fraction of regenerated production in Section 2. Surface temperature starts to increase in early spring (February-March) from a winter minimum of ≈12 °C and reached an annual maximum of ≈24 °C in August, a two-fold increase (see Fig. 6e) following the increase in solar radiation, with a temporal lag of two months. This temporal lag is due to the water's high thermal capacity. Note that the smooth seasonal dynamics of PAR at Blanes Bay shown in Fig. 6f was computed using astronomical functions because the in-situ measurements were extremely noisy due to the low frequency of sampling and stochastic cloud coverage (see Section 2). The (noisy) in-situ measurements of PAR are nevertheless consistent with the astronomical estimation (see Fig. 6f).

The seasonality of the chla-to-carbon ratio follows relatively well the seasonality of solar irradiance. The chla-to-carbon ratio displays a seasonal cycle with maximum values in winter (0.03 mg mg^{-1}) and minimum values in summer (0.01 mg mg^{-1}) (see Fig. 6d). This is because with high irradiance, phytoplankton cells can synthesize less chla per carbon and still perform photosynthesis unlimited by solar radiation. In other words, when light is saturating, cells need less chla molecules per carbon biomass to absorb enough light to saturate the carboxylation process. The seasonality of chla displays a factor of x4 change from ≈1.0 mg m^{-3} in winter (February) to ≈0.25 mg m^{-3} in summer (July), see Fig. 6g. With the total phytoplankton carbon estimated from species cell counts and size in combination with the 14C measured primary production, we computed the biomass-specific phytoplankton growth rate. With an average value of ≈0.6 d^{-1}, the growth rate shows a very weak seasonality, with phytoplankton growing slightly faster in late winter and autumn (see Fig. 6h). Primary production is higher in early spring (March) and lower in late summer (August), and displays a stronger seasonality (on the order of factor of x3) than the biomass-specific growth rate of phytoplankton. The primary production rates varies between ≈3.0 in spring and ≈1.0 mmolC m^{-3} d^{-1} in summer (see Fig. 6i).

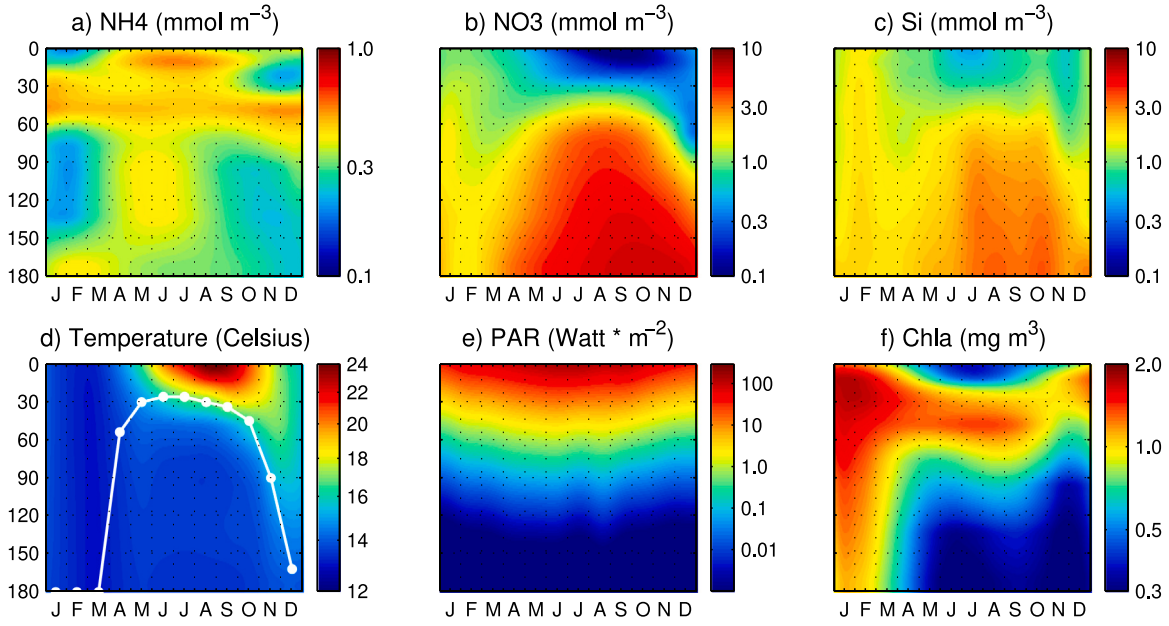

Fig. 3. Seasonal depth-resolved climatology of several environmental variables and phytoplankton chlorophyll-a at the Blanes Canyon station (Operational Observatory of the Catalan Sea; OOCS): (a) ammonium (mmol m^{-3}), (b) nitrate (mmol m^{-3}), (c) silica (mmol m^{-3}), (d) sea temperature (Celsius) and mixed layer depth (MLD), (e) photosynthetic active radiation (W m^{-2}), (f) chlorophyll-a (mg m^{-3}).

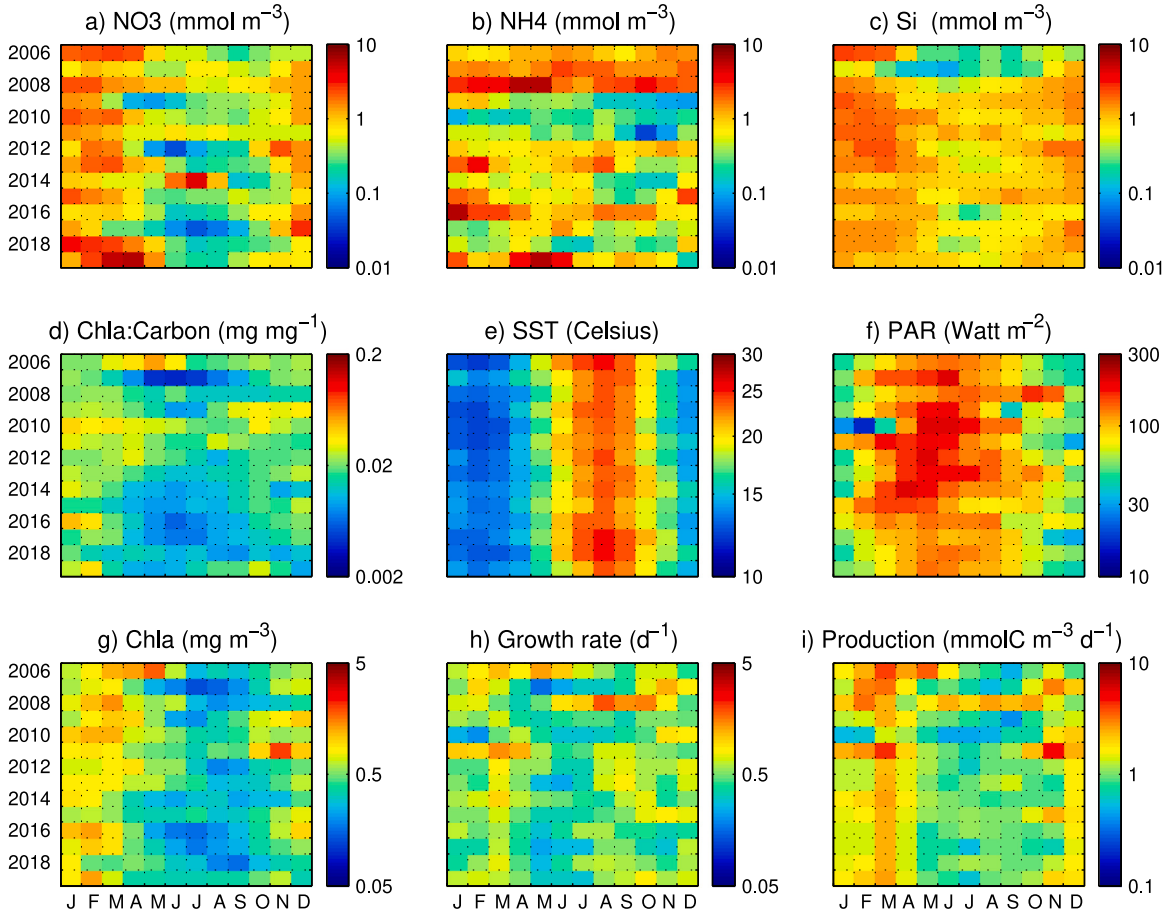

Fig. 4. Monthly averaged data per year of several environmental and biological variables at the Blanes Bay station (Blanes Bay Microbial observatory; BBMO): (a) nitrate (mmol m^{-3}), (b) ammonium (mmol m^{-3}), (c) silica (mmol m^{-3}), (d) Chla to Carbon ratio (mg mg^{-1}), (e) sea surface temperature (Celsius), (f) photosynthetic active radiation (W m^{-2}), (g) chlorophyll-a (mg m^{-3}), (h) growth rate (d^{-1}), (i) primary production (mmolC m^{-3} d^{-1}).

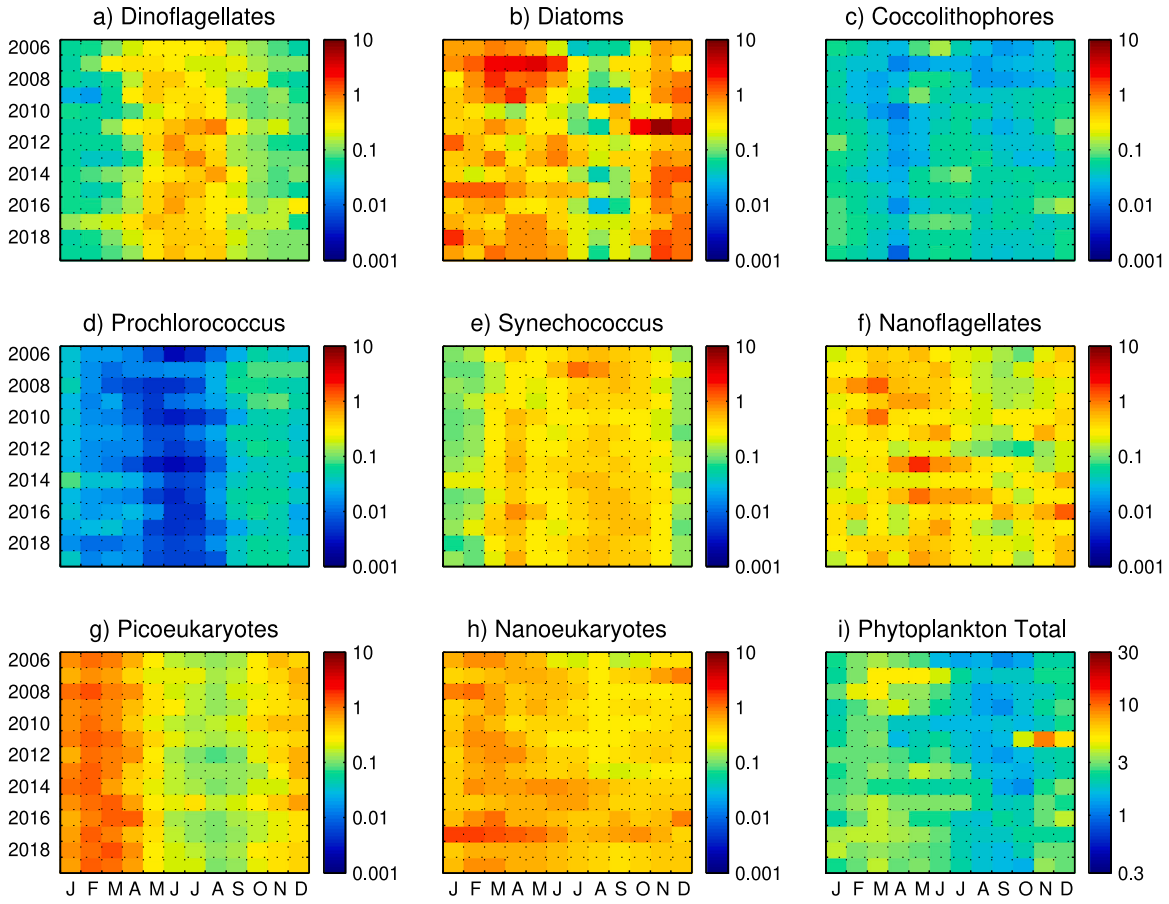

Fig. 5. Monthly averaged data per year of the phytoplankton biomass (mmolC m^{-3}) for the major phytoplankton groups at the Blanes Bay station: (a) Dinoflagellates, (b) Diatoms, (c) Coccolithophores, (d) Prochlorococcus, (e) Synechococcus, (f) Nanoflagellates, (g) Picoeukaryotes, (h) Nanoeukaryotes, (i) Phytoplankton Total. Biomass was computed based on the species' cell biovolume and an allometric carbon density factor (see Methods for details).

Fig. 4 shows the monthly averaged data per year for several environmental and biological variables, and Fig. 5 shows the same type of averaged data per year of the phytoplankton biomass (mmolC m^{-3}) for the major phytoplankton groups. There is a marked seasonality of the groups of phytoplankton present at Blanes Bay and the environmental conditions that affect them. One of the most clear patterns is that dinoflagellates concentration is highest when nutrient concentration is lowest, suggesting that dinoflagellates may be doing predatory mixotrophy on other phytoplankton groups. The seasonality of all variables can be better captured when plotting these data along with their climatological curves (see Figs. 6–8). Diatoms is the only phytoplankton group with high dispersion around their seasonal climatology (i.e. high interannual variability), due to their opportunistic nature and the low-resolution sampling frequency (see Fig. 7). Environmental factors tend to display a larger variance than the phytoplankton groups, with the exception of water temperature (see Fig. 6e). However, specially for nutrients, this can also be partly due to the low-resolution sampling frequency combined with spatial variability at the micro-scale (Vallina et al., 2019).

Total chlorophyll-a (Fig. 6g) shows a similar seasonality and variance as the total phytoplankton biomass (Fig. 7i). Total primary production (6i) shows a similar seasonality as total phytoplankton biomass (Fig. 7i) but with a larger variance. Biomass-normalized primary production gives a measure of phytoplankton growth rate or specific productivity (d^{-1}), and shows the lowest seasonality and the largest variance of the whole set of variables. Nevertheless, the seasonal patterns are generally robust for phytoplankton groups, the environmental factors, chla, primary production and phytoplankton productivity (see Figs. 7 and 6).

There are four phytoplankton groups with a particularly strong seasonal cycle, roughly between a maximum value of 1.0 mmolC m^{-3} and a minimum value of 0.1 mmolC m^{-3}: dinoflagellates, diatoms, *Synechococcus*, and picoeukaryotes. This means a factor of x10 change from peak to valley for their seasonal dynamics, although with out-of-phase signals among them. These four phytoplankton groups are the largest contributors to total phytoplankton, both in biomass and in seasonal variance. Dinoflagellates show a marked seasonal pattern with low interannual variability (see Fig. 7a). They have a mid summer maximum of 1.0 mmolC m^{-3} and a winter minimum of less than 0.1 mmolC m^{-3}. Diatoms show also a marked seasonal pattern but with high interannual variability (see Fig. 7b). They have a late winter/spring maximum of about 1.0 mmolC m^{-3} and a late summer/autumn minimum of about 0.1 mmolC m^{-3}. Diatoms show a particularly high dispersion around their seasonal climatology and show a quite low biomass minimum in summer, an order of magnitude lower than their winter maximum. Diatoms are almost but not perfectly in a complete out-of-phase seasonal signal when compared to dinoflagellates.

Synechococcus show a clean seasonal pattern with low dispersion around their seasonal climatology (i.e. low interannual variability). They have a spring first-peak maximum of 1.0 mmolC m^{-3}, followed by a moderate decrease down to 0.5 mmolC m^{-3} for two months (May, June), and then a long second dome-like maximum during summer of 1.0 mmolC m^{-3} again. The *Synechococcus* phylotypes forming the spring peak are known to be different than those forming the summer peak (Auladell et al., 2019). The annual minimum of 0.1 mmolC m^{-3} is observed during the winter months (see Fig. 7f). Picoeukaryotes have a marked seasonal pattern with the lowest interannual variability (see

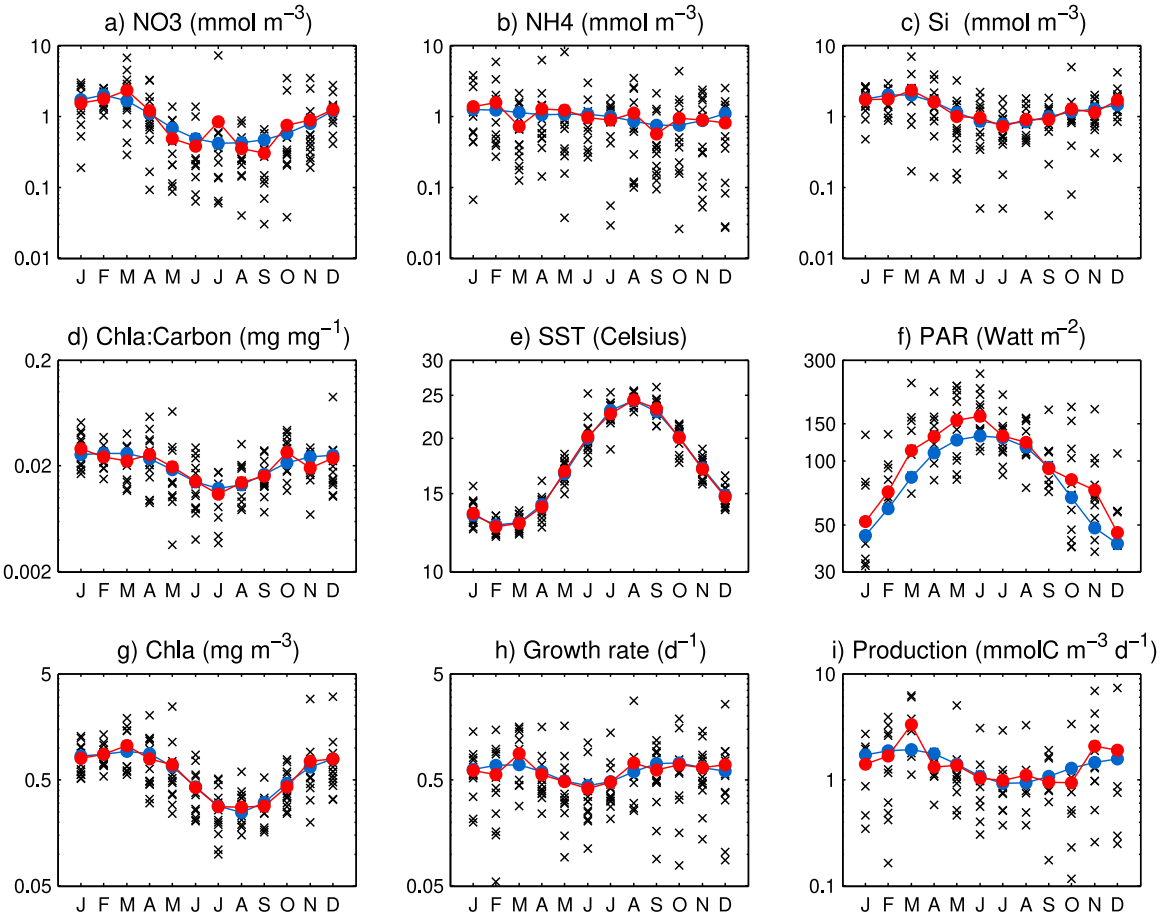

Fig. 6. Seasonal dynamics of several environmental and biological variables at the Blanes Bay station: (a) nitrate (mmol m^{-3}), (b) ammonium (mmol m^{-3}), (c) silica (mmol m^{-3}), (d) Chla to Carbon ratio (mg mg^{-1}), (e) sea surface temperature (Celsius), (f) photosynthetic active radiation (W m^{-2}), (g) chlorophyll-a (mg m^{-3}), (h) growth rate (d^{-1}), (i) primary production (mmolC m^{-3} d^{-1}). The black crosses are the raw data. The red curve are the monthly averages. The blue curve is the climatology obtained by fitting the data using harmonics regression, keeping only the first two harmonics.

Fig. 7g). They have an early spring maximum of 1.0 mmolC m^{-3} and a late summer minimum of 0.1 mmolC m^{-3}. Picoeukaryotes are in perfect and complete out-of-phase seasonal signal when compared to dinoflagellates. Nanoeukaryotes are also a major contributor to total phytoplankton biomass but not as much to seasonal variance (see Fig. 7h). Nanoeukaryotes have clear but weaker seasonal cycle, with sustained high levels of biomass. They have a long spring maximum of near 1.0 mmolC m^{-3} and a long autumn minimum of about 0.5 mmolC m^{-3}. This means a factor of x2 change from peak to valley for the seasonal dynamics of nanoeukaryotes, five times lower than for the previous four phytoplankton groups. These two groups (picoeukaryotes and nanoeukaryotes) encompass many phylogenetically diverse groups that have contrasting seasonality (Giner et al., 2019). Photosynthetic nanoflagellates have a clean seasonal cycle, with low dispersion around their seasonal climatology. Biomass levels are moderate, with similar upper and lower limits to those of *Synechococcus* (see Fig. 7f). Photosynthetic nanoflagellates have a spring maximum below 1.0 mmolC m^{-3} and autumn minimum above 0.1 mmolC m^{-3}. Therefore, their contribution to total biomass and seasonal variance is moderate.

Coccolithophores and *Prochlorococcus* have a seasonal cycle with low interannual variability (see Fig. 7c and d). However, their biomass is on average ten times lower than for the nanoflagellates group, being roughly between a maximum value of 0.1 mmolC m^{-3} and a minimum value of 0.005 mmolC m^{-3}. Coccolithophores has rather bimodal seasonal cycle. It starts with maximum values of 0.1 mmolC m^{-3} during winter, then a fast drop to an annual minimum value of less than 0.01 mmolC m^{-3} in spring (April), followed by a sudden increase to maximum values of 0.1 mmolC m^{-3} during summer, and finally a moderate decrease to values of the order of 0.05 mmolC m^{-3} during autumn (see Fig. 7c). *Prochlorococcus* has in contrast a clearer and well behaved seasonal cycle with low interannual variability. They have an autumn maximum of 0.1 mmolC m^{-3} and a summer minimum of 0.005 mmolC m^{-3} (see Fig. 7d). Note that our group of photosynthetic nanoflagellates are all cells larger than 5 μm (ESD) that could be detected by epifluorescence. The groups (pico, nano) eukaryotes are categories delimited by flow cytometry: the picoeukaryotes for sizes 1-3 μm; and the nanoeukaryotes for sizes 3–5 um. In winter, the dominant group is the smallest picoeukaryotes (chlorophytes, such as Ostreococcus, Micromomas). In summer, the dominant group is larger in size, basically haptophytes (Nunes et al., 2018). Since there is potential for somehow unclear overlap between (pico, nano) eukaryotes and photosynthetic nanoflagellates, we restricted our analysis to the largest size fraction of photosynthetic nanoflagellates (above 5 μm in ESD). The smallest size fraction of photosynthetic nanoflagellates (below 5 μm in ESD) was measured but not included in our analyses, due to the risk of excessive overlap with the (pico, nano) eukaryotes size fractions. The seasonality of the largest size fraction of photosynthetic nanoflagellates group is quite different from the seasonality of (pico, nano) eukaryotes, which suggests that the overlap must be minor. The contribution of photosynthetic nanoflagellates to total phytoplankton biomass is of a similar other of magnitude as the contribution of (pico, nano) eukaryotes, but nanoflagellates never dominate the phytoplankton community.

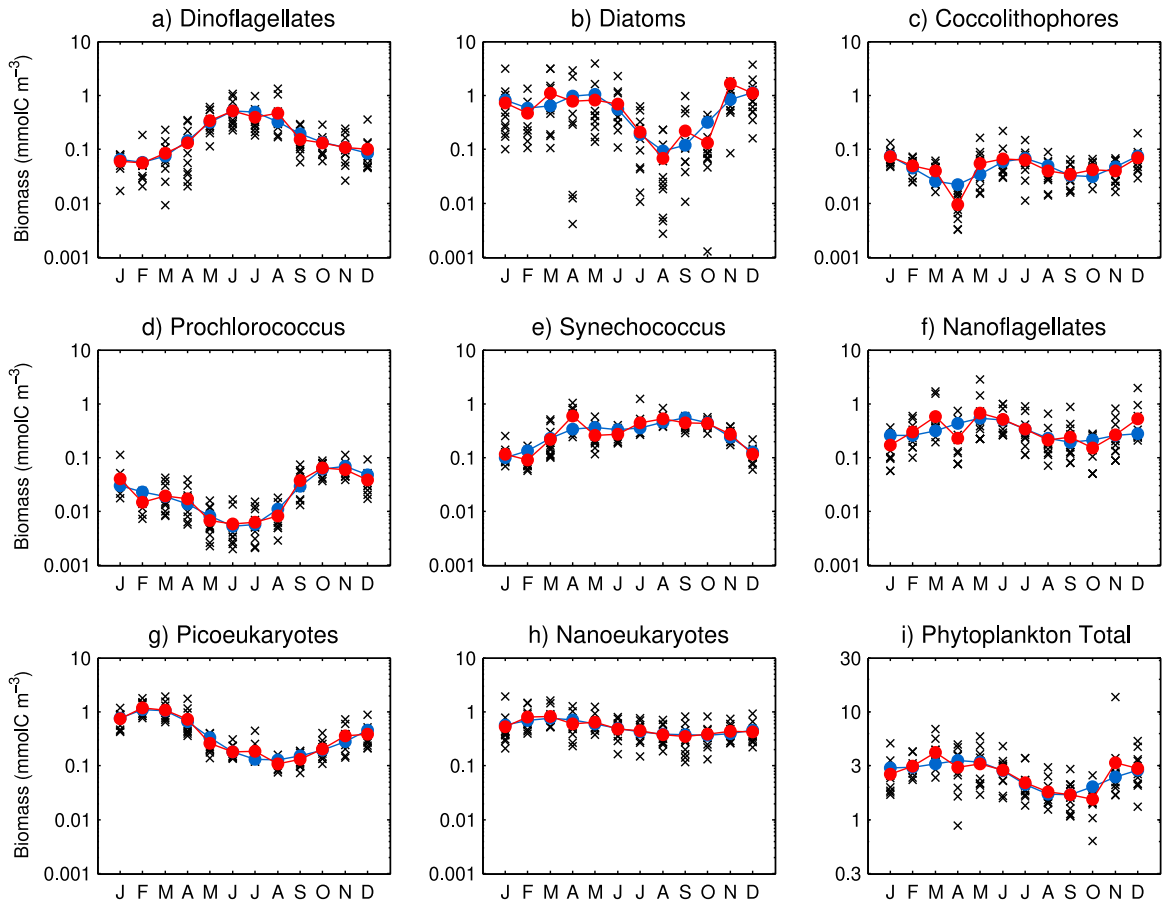

Fig. 7. Seasonal dynamics of the phytoplankton biomass (mmolC m^{-3}) for the major phytoplankton groups at the Blanes Bay station: (a) Dinoflagellates, (b) Diatoms, (c) Coccolithophores, (d) Prochlorococcus, (e) Synechococcus, (f) Nanoflagellates, (g) Picoeukaryotes, (h) Nanoeukaryotes, (i) Phytoplankton total. The black crosses are the raw data. The red curve are the monthly averages. The blue curve is the climatology obtained by fitting the data using harmonics regression, keeping only the first two harmonics.

The (annually averaged) relative contribution of each phytoplankton group to total phytoplankton biomass varies between less than 5% for coccolithophores and *Prochlorococcus* to more than 20% for all other groups (see Fig. 8). However, while dinoflagellates, diatoms and *Synechococcus* display large seasonal changes in their relative biomass (from less than 5% to more than 40%), nanoflagellates, picoeukaryotes and nanoeukaryotes display a smaller seasonality in their relative biomass (from 10% to 30%). Total phytoplankton biomass shows a clear seasonal pattern with moderate interannual variability, having a spring maximum of near 4.0 mmolC m^{-3} and a late summer minimum of 1.2 mmolC m^{-3} (see Fig. 7i). This means a factor of x3 change from peak to valley for the seasonal dynamics of total biomass. The highest total biomass for most of the years is observed in March, while the lowest biomass values tend to be observed during August, September, and October (see Fig. 5i). Although phytoplankton biomass displays its minimum with 1.2 mmolC m^{-3} in summer, the biomass increase again in late autumn with a secondary peak of 3.0 mmolC m^{-3}. This secondary peak in total biomass is mostly due to diatoms. During spring favorable conditions (high nutrients, high mixing, increasing light) allow a fast increase in diatom biomass (i.e. the spring bloom), going from a minimum value of 0.5 mmolC m^{-3} in February to a maximum value of 1.0 mmolC m^{-3} in just over a month (March). Therefore, the seasonal dynamics of total phytoplankton biomass and primary production seem to respond quite canonically to the wintertime nutrient supply combined with the spring-time increase in solar radiation. However, each group has a clear environmental niche (see Section 3.5) and thus they all display a different and distinct seasonality which makes them unique. This seasonal succession of phytoplankton groups tends to repeat itself every year in a regular fashion, being the seasonal variability of the phytoplankton groups larger than their interannual variability. Using one-way ANOVA, we computed the fraction of total variability explained by the interannual variability for each phytoplankton group. The contribution of interannual variability (between-years variance) to total variability is between 1.5% and 25%, with a median value of 7.5% and a mean value of 10%. That is, the contribution of seasonal variability (within-years variance) to total variability is between 75% and 98.5%, with a median value of 92.5% and a mean value of 90%. The fact that seasonal variability is much larger than the interannual variability, may partly be due to the still relatively short duration of the BBMO time series from the point of view interannual dynamics.

Figs. 9 and 10 provide an estimate for each phytoplankton group of their primary production and their biomass-specific growth rate, respectively. We used Eq. (21) described in Section 2. As expected, primary production (Fig. 9) shows similar seasonality as phytoplankton biomass (Fig. 7). However, the relative contribution to total primary production of each phytoplankton group is not simply equal to their relative contribution to total biomass (see Eq. (22)), otherwise each group would have exactly the same biomass-specific growth rate as all others, which is unlikely given their very different seasonal dynamics. Our estimates (see Eq. (21)) suggest that each phytoplankton group has a distinct seasonal pattern in biomass-specific growth rate as a function of the environmental conditions. Only three groups have their seasonally highest growth rates reaching ≈1.0 (d^{-1}): diatoms (in spring and autumn), *Synechococcus* (in late summer), picoeukaryotes (in winter); and only two groups have their seasonally highest growth

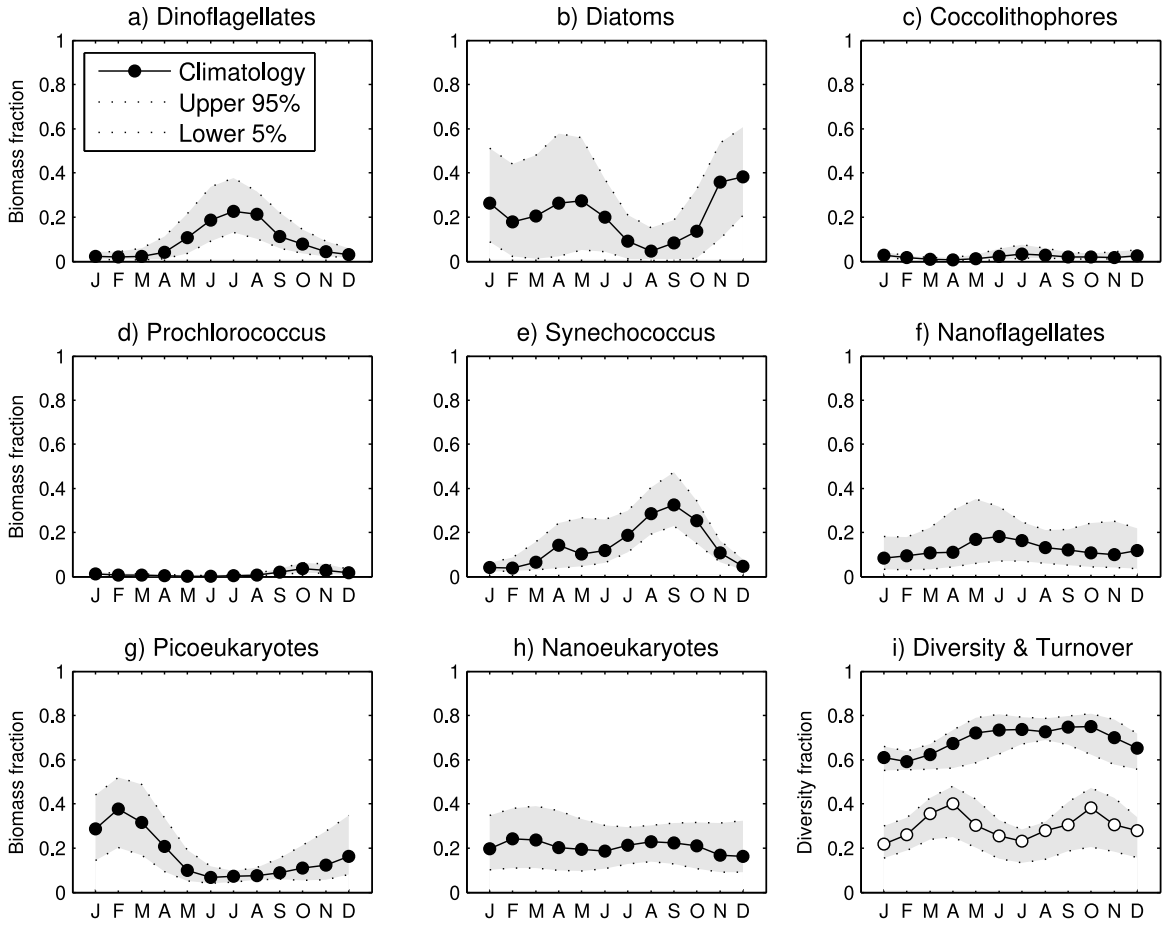

Fig. 8. Seasonal dynamics of the relative contribution to total phytoplankton biomass (n.d.) for the major phytoplankton groups at the Blanes Bay station: (a) Dinoflagellates, (b) Diatoms, (c) Coccolithophores, (d) Prochlorococcus, (e) Synechococcus, (f) Nanoflagellates, (g) Picoeukaryotes, (h) Nanoeukaryotes; Seasonal dynamics of (i) Phytoplankton group α-diversity (black dots) and phytoplankton group turnover (white dots). Phytoplankton group α-diversity was computed as the exponential of the Shannon index and then normalized by its maximum potential richness (eight phytoplankton groups). Phytoplankton group turnover was computed as the (1 - β-diversity) between sequential samples that are one month apart in temporal distance (time lag = 1 month). Phytoplankton group β-diversity was computed as the Bray–Curtis similarity index. The gray shadow displays the dispersion of the data. The solid curve is the climatology obtained by fitting the data using harmonics regression, keeping only the first two harmonics. The dotted curves are the upper (percentile 95%) and lower limits (percentile 5%).

rates below 0.2 ≈ 1.0 (d^{-1}): coccolithophores and *Prochlorococcus*. The other three groups have their seasonally highest growth rates between ≈0.2 and ≈0.8 (d^{-1}): nanoeukaryotes (in late winter and late summer), dinoflagellates (in summer), and nanoflagellates (in autumn). The primary production and growth rates for the whole phytoplankton community was compared to the monthly means computed from the observational raw data (see Figs. 9i and 10i).

3.3. Validation

We compare our carbon biomass concentration estimates for the different phytoplankton groups to alternative estimates based on pigments and the CHEMTAX algorithm (Nunes et al., 2018). The climatological estimates of chla for the several phytoplankton groups described in Nunes et al. (2018) were converted to phytoplankton biomass using Eq. (18) and compared to our estimates (see Fig. 11). The phytoplankton groups defined with CHEMTAX only match partially our taxonomically defined groups, being only five of them explicitly the same groups for both approaches: dinoflagellates, diatoms, coccolithophores (Haptophytes), *Prochlorococcus*, *Synechococcus*. All of them show a good agreement between both approaches, with the notable exception of the group coccolithophores (Haptophytes). Our group picoeukaryotes does also compare well to the CHEMTAX group of Prasinophytes, and our group nanoeukaryotes has a similar seasonality as the CHEMTAX group of Cryptophytes but one order of magnitude difference in carbon biomass concentration. Note that we plotted our group nanoflagellates together with the CHEMTAX group of Pelagophytes only for graphical purposes.

Using the environmental conditions as external forcing (seawater temperature, solar irradiance, nutrient concentration) the seasonal dynamics of several biological variables at BBMO was simulated using a diagnostic approach (see Section 2 for details). Chla and sea temperature are directly measured variables, while chla-based biomass and primary production are modeled using the equations described in Table 1. The modeled estimates for chla-based biomass, primary production, chla-to-carbon ratio, and specific growth rate were then validated against their corresponding climatologies constructed from observed data at BBMO (abundance-based biomass, 14C primary production, chla-to-carbon ratio, and specific growth rate), showing good agreement between the two approaches (see Fig. 12). This diagnostic modeling approach allow us to obtain an estimate of the fraction of regenerated production by phytoplankton at BBMO. The results show that primary production at Blanes Bay is partially sustained by regenerated production from ammonium uptake, with (1 - f_{ratio}) values between 40% in late-autumn and 60% in summer (see Fig. 13). This implies that the fraction of new production from NO3 uptake (the f_{ratio}) is quite high throughout the year (40%–60%), possibly reflecting the influence of upwelling. This is especially so considering that ammonium can

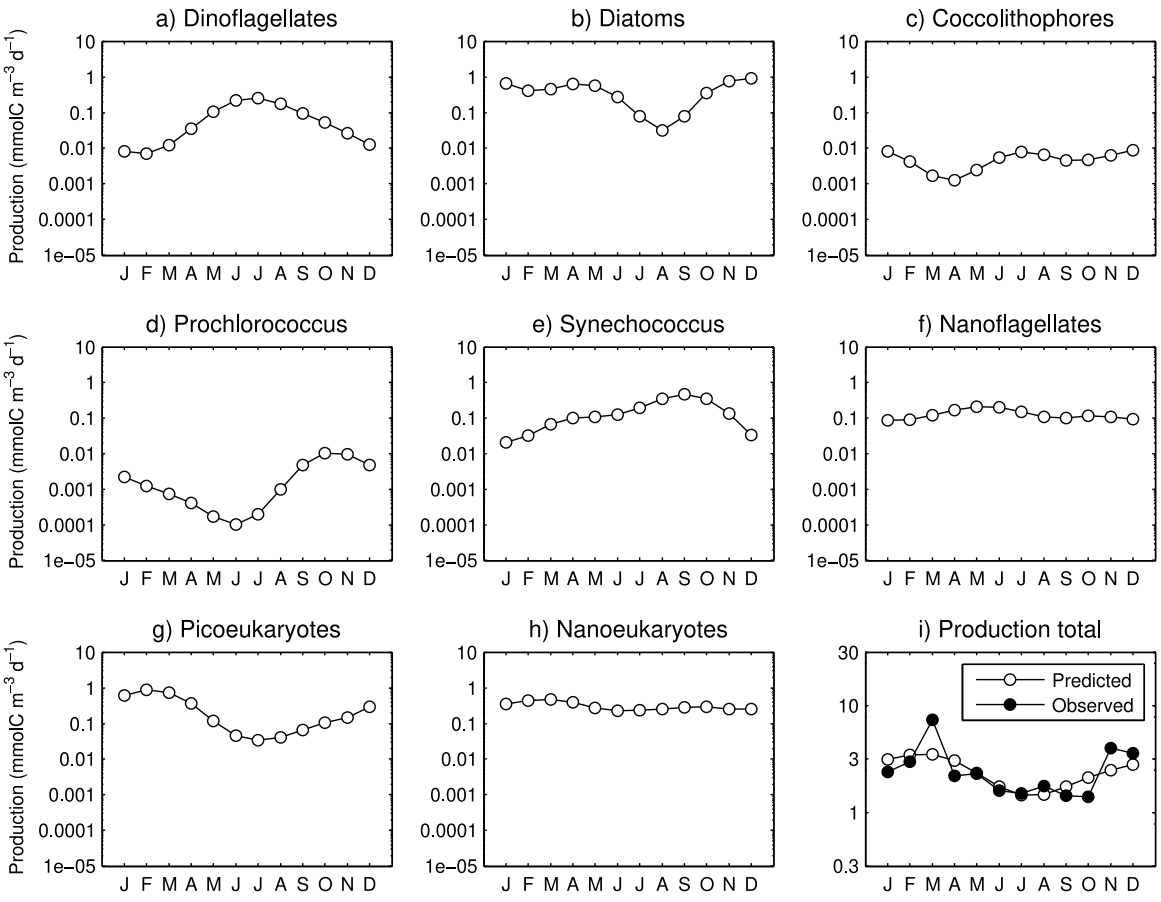

Fig. 9. Seasonal dynamics of the phytoplankton production (mmolC m^{-3} d^{-1}) for the major phytoplankton groups at the Blanes Bay station: (a) Dinoflagellates, (b) Diatoms, (c) Coccolithophores, (d) Prochlorococcus, (e) Synechococcus, (f) Nanoflagellates, (g) Picoeukaryotes, (h) Nanoeukaryotes, (i) Phytoplankton total. These values were estimated using the climatological time-series from the harmonics regression fit to the raw biomass data (see Methods for details).

inhibit NO3 uptake. Regenerated production from ammonium uptake (1 - f_{ratio}) can reach 80%–90% in oligotrophic regimes such as BATS in summer (Martin and Pondaven, 2006).

3.4. Mean cell size

Figs. 14 and 15 provide information regarding the cell size distribution of the phytoplankton community at BBMO. The upper panels in Fig. 14 show the climatology of the mean cell size (a) and the standard deviation of cell size (b), computed on the log-scale ESD distributions of cell abundance (white dots) and of carbon biomass (black dots). Cell size average was computed as the weighted mean, either by biomass or abundance, of the log-scale ESD distributions. The standard deviation of a log-scale ESD distribution is a metric of the diversity of cell sizes that are present in the phytoplankton community (Acevedo-Trejos et al., 2015; Smith et al., 2016). The mean cell size of the phytoplankton community tends to decrease from winter to late summer, and this is specially clear when using cell abundance as the weights for computing the average. When using carbon biomass as weights for the average, however, there are two annual peaks in mean cell size: in winter and in late spring. The increase of mean cell size in winter is due to diatoms, while the increase in late spring is due to both dinoflagellates and diatoms. These two groups have the largest cell sizes of all groups (see Fig. 2a) and their contribution to the biomass-weighted mean ESD of the whole community follows their time-series. During late summer, the community is dominated by small phytoplankton such as nanoeukaryotes and *Synechococcus*, either using cell abundance or carbon biomass when computing the weighted mean ESD.

The standard deviation of cell size (or ESD sigma) tends to decrease from winter to late summer when using cell abundance as weights, but this trend is not observed when using carbon biomass as weights (see Fig. 14b). However, the seasonality of ESD sigma (i.e. size diversity) is relatively weak in either case (1.33 fold change from valley to peak). Size diversity (using biomass as weights) displays a similar seasonality as α-diversity at the phytoplankton group level, being highest during summer and lowest during winter (see Figs. 14b and 8i; black dots). The lower panels in Fig. 14 show the relationship between the standard deviation of cell size versus the mean cell size (c) and species diversity (d) using the whole set of interannual monthly observations. Species diversity was computed as the exponential of the Shannon index or *effective richness* (MacArthur, 1965; Jost, 2006; Vallina et al., 2017). Two clear patterns can be observed: 1. the relationship between cell size diversity and mean cell size is unimodal, with cell size diversity peaking at intermediate values of mean cell size (8 μm); 2. there is a positive relationship between cell size diversity and species diversity, which implies that cell size diversity can indeed be a good proxy of functional diversity as previously suggested (Acevedo-Trejos et al., 2015).

The upper panels in Fig. 15 show the relationship between primary production versus chla (a) and carbon biomass (b). The lower panels show the relationship between primary production (c) and carbon biomass (d) versus mean cell size computed on the log-scale ESD distributions of carbon biomass. Primary production is positively correlated (Pearson's ρ) to both chla (ρ = 0.43) and to carbon biomass (ρ = 0.43). Primary production is also positively correlated to mean cell size but this relationship is weaker (ρ = 0.30). This implies that higher

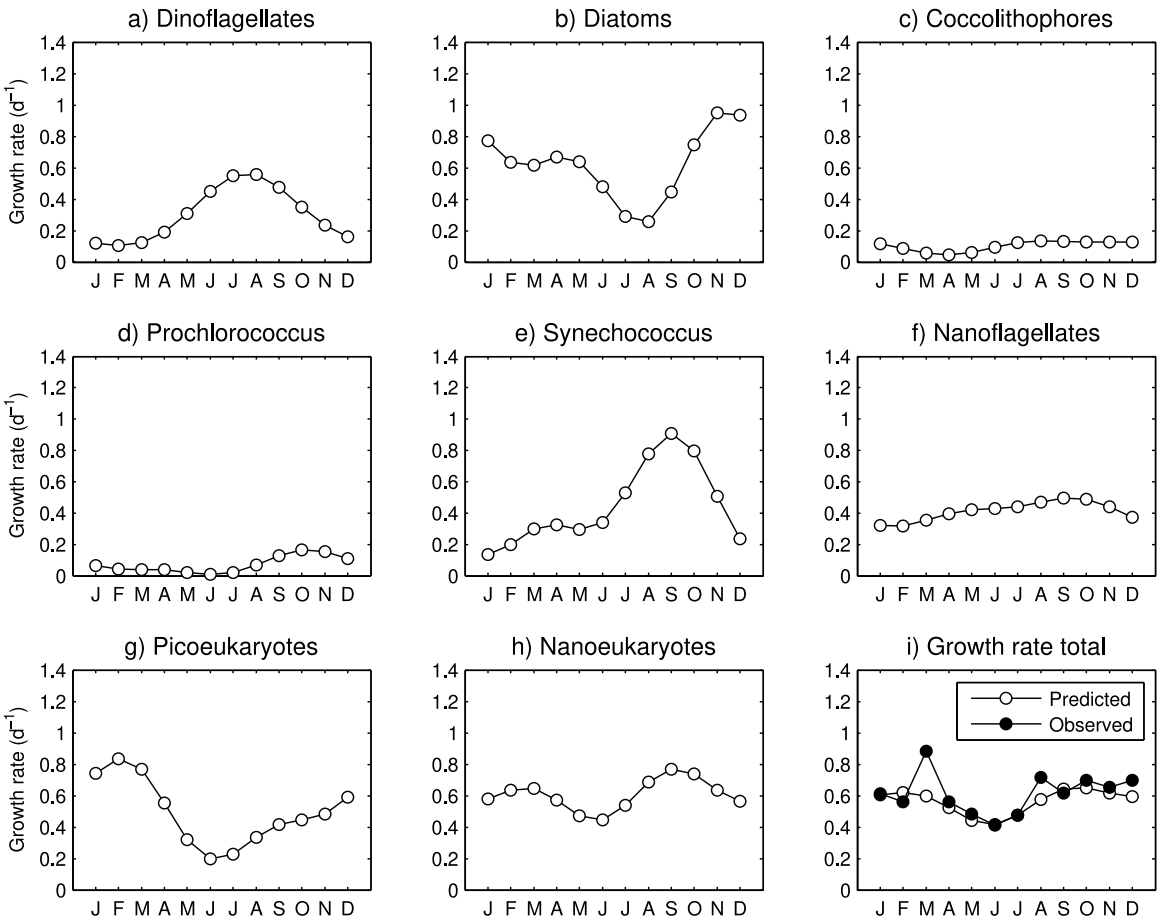

Fig. 10. Seasonal dynamics of the phytoplankton growth rate (d^{-1}) for the major phytoplankton groups at the Blanes Bay station: (a) Dinoflagellates, (b) Diatoms, (c) Coccolithophores, (d) Prochlorococcus, (e) Synechococcus, (f) Nanoflagellates, (g) Picoeukaryotes, (h) Nanoeukaryotes, (i) Phytoplankton total. These values were estimated using the climatological time-series from the harmonics regression fit to the raw biomass data (see Methods for details).

values of primary production tend to occur when larger cells dominate the phytoplankton community (Marañón, 2015) but there is a lot of dispersion around the linear trend. Carbon biomass is actually better correlated to mean cell size than primary production ($\rho = 0.40$). That is, larger values of carbon biomass also tend to occur when larger cells dominate the phytoplankton community (Marañón, 2015).

3.5. Ecological niches

Fig. 16 show the rank abundance (here biomass) distributions (RAD) of the 8 phytoplankton groups at Blanes Bay using their climatological time-series. The climatology is based on data fitting using first-two harmonics regression, which provides the same curves as using the monthly means with a more smooth signal (compare the red curves versus the blue curves in Figs. 6 and 7). There is a clear alternation in dominance depending the month of year for five of the phytoplankton groups: diatoms, dinoflagellates, picoeukaryotes, nanoeukaryotes, and *Synechococcus*. Photosynthetic nanoflagellates does contribute moderately to total biomass but never raise to dominance (see Fig. 8), being always between the third and fifth position (see Fig. 16). The other two phytoplankton groups, however, do never raise beyond being rare: coccolithophores, and *Prochlorococcus*. Yet, even these *rare-biosphere* (Pedros-Alio, 2012) groups alternate their rank position depending on the month of year. Most of the months, the dominant phytoplankton groups are relatively even in their biomass, with the exception of November and December when diatoms clearly dominate the phytoplankton community (see Fig. 8). The least dominant phytoplankton groups tend to consistently be coccolithophores and *Prochlorococcus*. This alternation in ranked position in time of the 8 groups implies that each phytoplankton groups has a characteristic environmental niche where they perform best. Fig. 17 shows the biomass of each phytoplankton group as a function of three major environmental factors known to affect phytoplankton growth: dissolved inorganic nitrogen, water temperature, and solar irradiance. Biomass was standardized using the z-score transformation (i.e. subtracting the mean and dividing by the standard deviation) in order to have a standard score value of zero mean and standard deviation equal to one. The niche location of each phytoplankton group is shown for the seasonal climatologies as coordinates in this 3D environmental trait space, while the corresponding colormap gives the z-score biomass of each phytoplankton group at each niche location. The point marking the beginning of each of the four seasons (winter, spring, summer, autumn) is over-imposed to help locate the temporal date corresponding to the 3D environmental coordinates. Different phytoplankton groups tend to dominate the phytoplankton community under different environmental niches, which correspond to different temporal locations within a climatological year (see Figs. 8, 16 and 17).

Dinoflagellates have their annual maximum at the beginning of summer, and thus when PAR is highest, SST is rising, and DIN are lowest due to over-consumption by the whole phytoplankton community. Dinoflagellates have their annual minimum at the beginning of winter, with the exact opposite environmental conditions. Diatoms have a clear annual minimum in late summer, where PAR is high but decreasing, temperature is highest, and nutrients are still quite low. Diatoms do not show a clear niche leading to a neat annual maximum, although

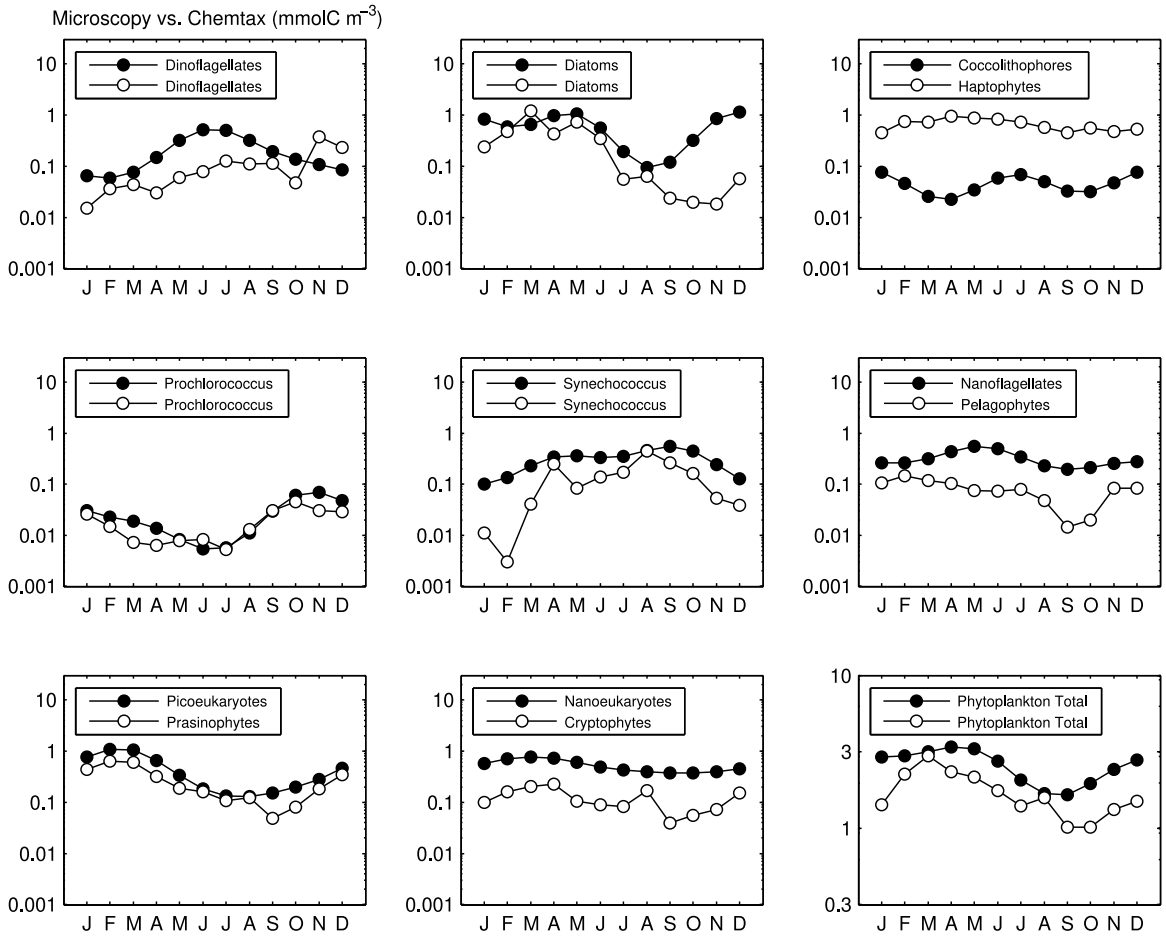

Fig. 11. Validation of the seasonal dynamics of the phytoplankton biomass (mmolC m^{-3}) for the major phytoplankton groups at the Blanes Bay station using pigment-based analysis (chemtax) from Nunes et al. (2018): (a) Dinoflagellates, (b) Diatoms, (c) Coccolithophores, (d) Prochlorococcus, (e) Synechococcus, (f) Nanoflagellates, (g) Picoeukaryotes, (h) Nanoeukaryotes, (i) Phytoplankton total. The black dots are the climatology obtained by fitting the data using harmonics regression, keeping only the first two harmonics. The white dots are the monthly averages from chemtax (Nunes et al., 2018).

they display high values during autumn and spring, and moderate values during winter. This reflects their opportunistic nature, and as long as nutrients are available they can grow (Nunes et al., 2018). Coccolithophores have a clear maximum in late autumn, when PAR is lowest, SST is decreasing, and DIN is highest. They also have a smaller secondary peak in late spring, when PAR is highest, SST are similar to those of the primary peak, and DIN is lowest. This is because there are different coccolithophores species, some associated to low irradiance while others associated to high irradiance (not shown). *Prochlorococcus* have an annual maximum during autumn, when PAR is decreasing, SST decreasing but still high, and DIN is increasing. They have an annual minimum during late spring/early summer, when PAR is highest, SST is increasing, and DIN is lowest.

Synechococcus have a clear annual minimum at the beginning of winter, when PAR is lowest, SST is decreasing, and DIN is highest. They have an annual maximum during late summer, when PAR is decreasing, SST is highest, and DIN is low. Nanoflagellates have an annual maximum in late spring or at the beginning of summer, when PAR is highest, DIN is low, and SST is increasing. They have an annual minimum during autumn, when PAR is decreasing, SST is still high, and DIN is moderate and increasing. Picoeukaryotes show an annual maximum in mid-winter, when PAR is low, SST is lowest, and DIN is high. They show an annual minimum during mid-summer with the exact opposite environmental conditions. Nanoeukaryotes show an annual maximum at the beginning of spring, when PAR is increasing, SST is lowest, and DIN is decreasing by consumption. They show an annual minimum at the beginning of autumn, with the exact opposite conditions for SST but similar conditions of PAR and DIN as their annual maximum. Finally, the total phytoplankton community has an annual maximum from winter to late spring, when PAR is increasing, SST is low, and DIN is high but decreasing by consumption. Total phytoplankton has an annual minimum during mid-summer, when PAR is high, SST is highest, and DIN is lowest due to consumption.

Maximum phytoplankton biomass is observed under relatively low nutrient concentration, intermediate solar radiation, and cold waters. However, it is important to point out that nutrients tend to be taken up relatively fast by the phytoplankton community, so that bulk nutrient concentration may not reflect appropriately the actual nutrient supply flux coming up from deep waters by turbulent mixing (Otero-Ferrer, 2020). Resource–consumer interactions (e.g. phytoplankton uptake on nutrients) can lead to uncorrelation between nutrient and phytoplankton dynamics if the time-lag between nutrient supply and phytoplankton uptake is shorter than the frequency of measurements. According to these results, we can conclude that phytoplankton groups at Blanes Bay appear to follow their specific ecological niches, tracking the seasonal changes in environmental conditions. We then performed a seasonal correlation analysis of the eight phytoplankton groups, the total phytoplankton community, and the three environmental variables (DIN, SST, PAR) all against all to obtain a correlation matrix (see Fig. 18a). We also show the individual z-score times-series used to compute the correlation matrix (see Figs. 18c and 18d) and the phase coupling among them of the first harmonic used to fit the data, which

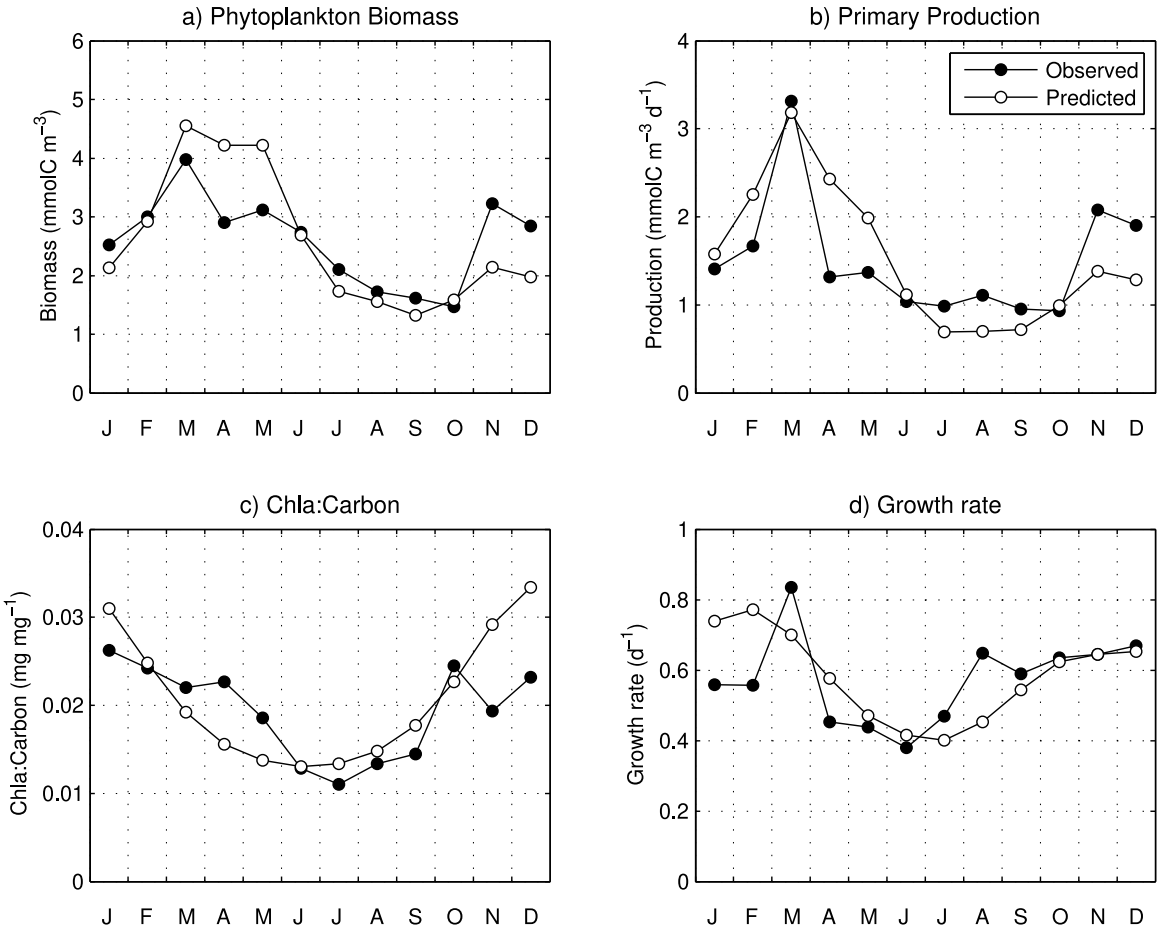

Fig. 12. Validation of the seasonal dynamics of several biological variables at the Blanes Bay station: (a) Phytoplankton total biomass (mmolC m^{-3}), (b) primary production (mmolC m^{-3} d^{-1}), (c) Chla to Carbon ratio (mg mg^{-1}), (d) growth rate (d^{-1}). The black dots display the observed climatology and the white dots display the predicted seasonality using a diagnostic model (see Methods for details).

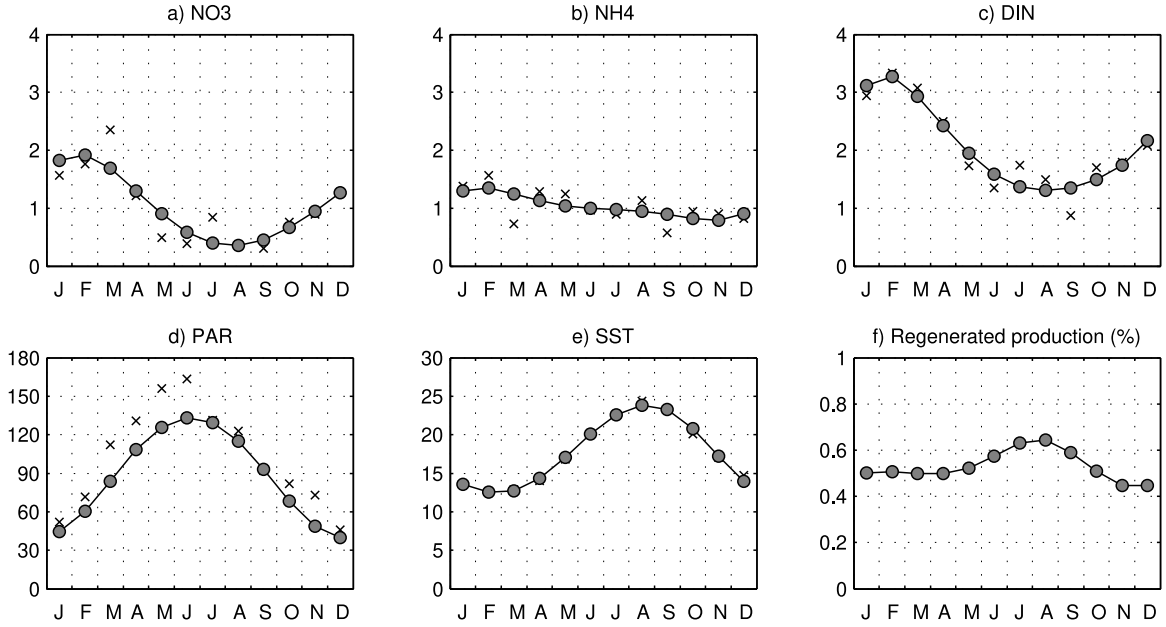

Fig. 13. Seasonal dynamics of several environmental variables needed to estimate regenerated primary production using a diagnostic model (see Methods for details) at the Blanes Bay station: (a) nitrate (mmol m^{-3}), (b) ammonium (mmol m^{-3}), (c) dissolved inorganic nutrients (NO3 + NH4), (d) photosynthetic active radiation (W m^{-2}), (e) sea surface temperature (Celsius), (f) fraction of regenerated production (n.d.). The black crosses are monthly averages. The gray dots display the climatology obtained by fitting the monthly-averaged data using harmonics regression, keeping only the first two harmonics.

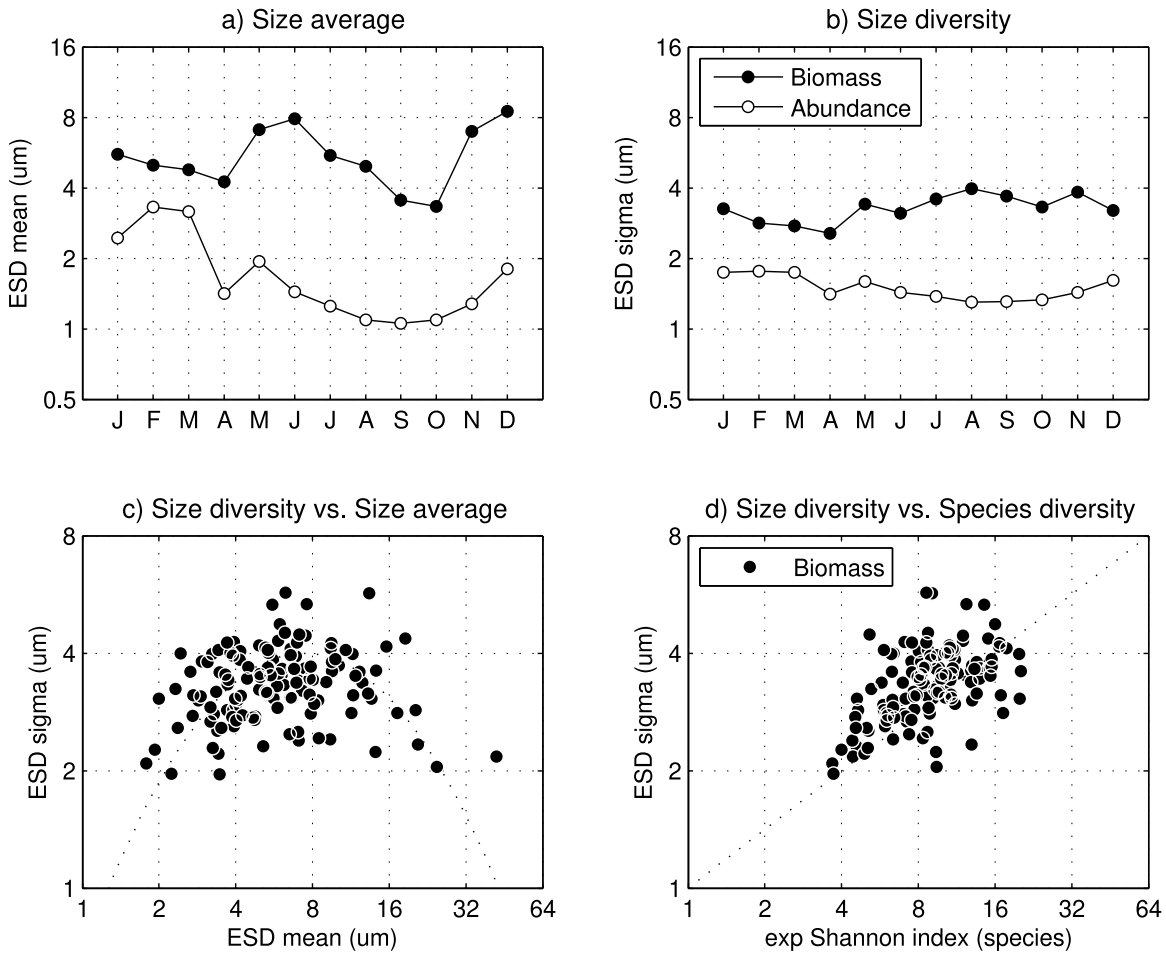

Fig. 14. Upper panels: Climatology of the mean cell size (a) and cell size diversity (b) computed on the equivalent spherical diameter (ESD) distributions (in log scale) using cell abundance (white dots) and carbon biomass (black dots). Lower panels: Relationship between cell size diversity versus mean cell size (c) and versus species diversity using the whole set of inter-annual monthly observations of the BBMO time-series. Mean cell size was computed as the weighted (by biomass or abundance) mean of log(ESD). Size diversity was computed as the standard deviation of log(ESD). Species diversity was computed as the exponential of the Shannon index.

is the dominant frequency (see Fig. 18b). This analysis shows that each phytoplankton group has a unique time-series and that the correlation value between time-series is driven by their level of phase coupling: $\delta(x, y) = \mid 0.5 - \Delta\theta \mid / 0.5$, where $\Delta\theta = \mid \theta_x - \theta_y \mid$ measures the distance between the phases (θ) of time-series signals $x(t)$ and $y(t)$. Exact phase coupling ($\delta = 1.0$) leads to highest positive correlation; phase decoupling ($\delta = 0.5$) leads to zero correlation; and phase uncoupling ($\delta = 0.0$) leads to highest negative correlation. This large variability in seasonal cycles of the phytoplankton groups at Blanes Bay is probably related to more environmental factors than the three used here to describe their ecological niche (DIN, SST, PAR). Therefore, further research should address this gap of knowledge regarding the other potential environmental dimensions affecting the ecology of phytoplankton groups at Blanes Bay (Dutkiewicz et al., 2020). Furthermore, these are patterns at the phytoplankton group level but some groups are phylogenetically coherent and others are not. It is unlikely that all the components of each group are governed by what governs the group as a whole. This also merits further research.

3.6. Dynamics of α-diversity and β-diversity

Fig. 19 shows the Bray–Curtis *similarity* index (β-diversity) of the phytoplankton communities as a function of the temporal lag between samples, both at the group level and at the species level. Note that only dinoflagellates, diatoms, and coccolithophores have their taxonomic composition resolved to the level of species here, they contribute with more than 300 species in total. However, *Prochlorococcus*, *Synechococcus*, picoeukaryotes, nanoeukaryotes, and nanoflagellates are too small to be classified to the species level using optical microscopy methods. Fig. 8i (white dots) shows its mirror index at the group level, the Bray–Curtis *dissimilarity* (1 - β-diversity), as a function of time within a climatological year for a time-lag of one month. This provides a measure of the seasonality of phytoplankton group replacement or temporal turnover from one month to the next one (Righetti et al., 2019). There is a clear pattern of two annual peaks of increased turnover of phytoplankton groups, one in spring and a second one in autumn. While the first pulse leads to a 1.33 fold increase in α-diversity, the second pulse leads to a similar decrease in α-diversity (see Fig. 8i; black dots). Therefore, α-diversity is highest during summer and lowest during winter; although it is quite high throughout the year, with values between 60% and 80% of its maximum potential richness of eight phytoplankton groups.

Fig. 19 reveals a long-term sinusoidal pattern associated with the seasonal recurrence of species occurrences. This has also been shown in the BBMO for (genetic) species of picoeukaryotes and nanoeukaryotes (both autotrophic and heterotrophic) and for heterotrophic prokaryotes (Giner et al., 2019; Auladell et al., 2019). Despite some large variability (dispersion) in the Bray–Curtis similarity, even for the longest time-lags, the analysis demonstrates a strong link between environmental conditions and taxonomic composition. This link emerges

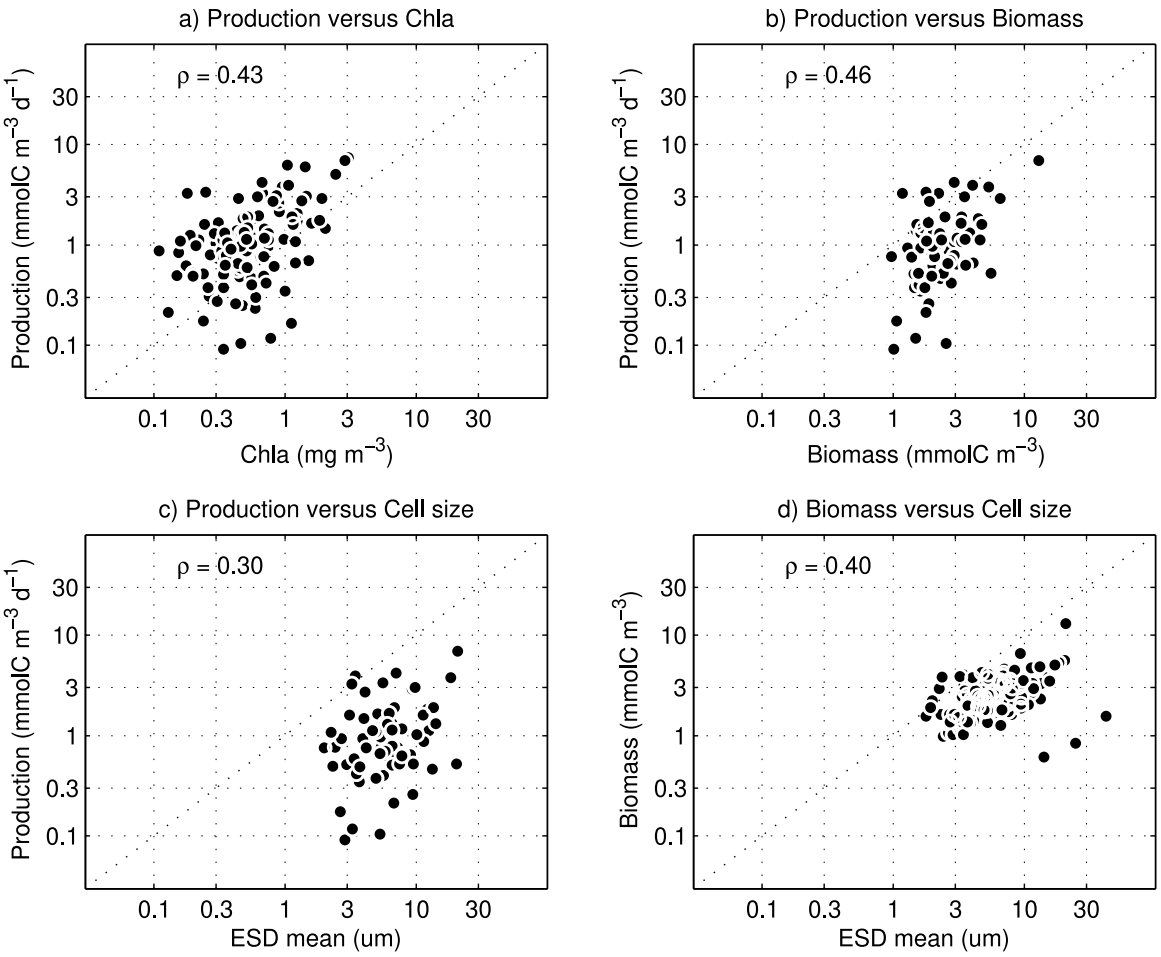

Fig. 15. Upper panels: Relationship between primary production versus chla (a) and carbon biomass (b). Lower panels: Relationship between primary production (c) and carbon biomass (d) versus mean cell size computed on the log(ESD) distributions of carbon biomass. All panels are using the whole set of inter-annual monthly observations of the BBMO time-series. The Pearson's correlation between variables is denoted as ρ.

regardless of whether the analysis is performed using data at the group or species level. We attribute it to a core of groups/species that appear consistently when their physiological characteristics match environmental conditions. The variability around the average trend is associated with the bulk of the rare species that prevail throughout the year. These species can eventually become dominant if the environmental conditions turn favorable for their growth (see Fig. 8). The long-term sinusoidal trend, indicative of seasonal variability in community similarity, prevails almost perfectly flat throughout the 12 years of the time series, reinforcing the idea that the assembly of these communities is largely governed by niche rules. To formally evaluate the validity of niche theory and neutral theory in predicting this observed seasonal pattern of temporal β-diversity at BBMO, we performed numerical simulations using the MIT Darwin model under a chemostat-bioreactor setup for two contrasting scenarios: (1) one assuming the niche theory dynamics; (2) and one assuming the neutral theory dynamics for the community assembly of 64 phytoplankton ecotypes. The description of the assumptions for both approaches (niche versus neutral) is given in Appendix. The niche theory simulation predicts a sinusoidal function of β-diversity with temporal distance between samples, while the neutral theory simulation predicts an exponential decay of β-diversity (community similarity) with temporal distance (time-lag) between samples (see Fig. 20).

4. Discussion

4.1. Physical environment

The vertical domain of this coastal site is shallow, going down to 20 m in depth (Guadayol et al., 2009). However, due to strong mesoscale circulation, the ecosystem dynamics of the inshore Blanes Bay station behaves similarly to the offshore station located in the Blanes canyon (Bahamon et al., 2011), which has a much deeper water column (>200 m). The water column in the BBMO is well mixed (vertically homogeneous) during autumn–winter and becomes stratified during summer when the MLD is located between 5 to 10 m (see Figure S1 in Nunes et al. (2018)). Dissolved inorganic nutrients are a factor of three higher in winter (≈3.0 mmolN m^{-3}) than in summer (≈1.0 mmolN m^{-3}), water temperature is a factor of two higher in summer (≈24 C) than in winter (≈12 C), and solar radiation is a factor of four higher in summer (≈140 W m^{-2}) than in winter (≈35 W m^{-2}) (see Fig. 13)

4.2. Phytoplankton chla

Phytoplankton chla (mg m^{-3}) observations at the surface in the coastal station BBMO vary seasonally between ≈1.0 in the spring bloom and ≈0.20 in summer (a factor of five decrease). These values are four times larger than the phytoplankton chla observed at the open-ocean station BATS, which vary seasonally between ≈0.25 in the spring

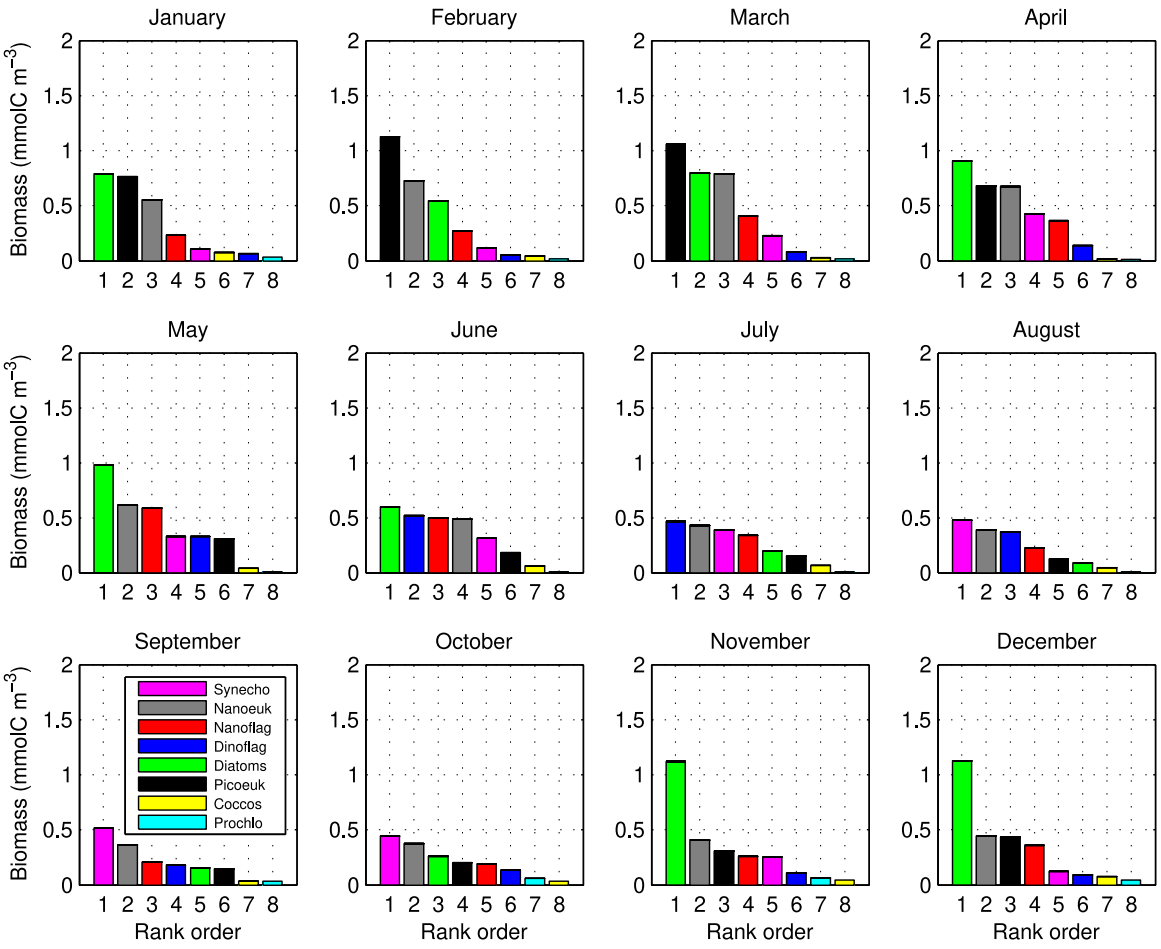

Fig. 16. Seasonal variability in the rank abundance (here biomass) distribution (RAD) of the phytoplankton group at the Blanes Bay station using their climatological time-series.

bloom and ≈0.05 in summer (a factor of five decrease) (Goericke and Welschmeyer, 1998; Vallina, 2008a). Coastal sites are known for being more productive than open-ocean locations because phytoplankton in these regions suffer less from nutrient limitation (Sigman and Hain, 2012; Huete-Ortega et al., 2014). In fact, primary production in coastal margins supports the vast majority of oceanic fisheries (Falkowski et al., 1998). Yet, the chla values at BBMO are similar to the chla observed at open-ocean station DYFAMED (annual mean of ≈0.30), also located in the NW Mediterranean Sea about 50 km offshore Nice (France) (Marty and Chiavérini, 2002). Chla concentration in DYFAMED varies seasonally between ≈1.0 in the spring bloom and ≈0.10 in summer (a factor of ten decrease) (Marty and Chiavérini, 2002; Marty et al., 2008). Therefore, part of the difference between BBMO and BATS results from their different latitude (41°67N for BBMO and 31° 50N for BATS) and because of the proximity of the Sargasso Sea to the oligotrophic gyre of the North Atlantic ocean.

4.3. Phytoplankton community biomass

We converted abundance to biomass using an allometric relationship of cell carbon density (pgC μm^{-3}) with cell volume (see Section 2 for details). This carbon density factor (CDF) decreases five-fold from a cell size of ESD = 0.5 μm to a cell size of ESD = 64 μm (see Figure), which is a size range that encompasses the lower and upper limits of the mean ESD for all phytoplankton groups. These values of cell carbon density are well within published values from laboratory estimates for different phytoplankton group (Verity et al., 1992; Menden-Deuer and Lessard, 2000; Montagnes and Franklin, 2001; DuRand et al., 2002; Segura-Noguera et al., 2012; Graff et al., 2012; Mcnair et al., 2021). Our seasonal estimates of total phytoplankton biomass (mmolC m^{-3}) from cell counts are similar to those based on chla (see Fig. 12). Phytoplankton biomass at BBMO vary seasonally from ≈4.0 in the spring bloom and ≈1.0 in summer (a factor of four decrease). These values are twice as large as the phytoplankton biomass estimates reported at BATS, which vary seasonally from ≈2.0 in the spring bloom and ≈0.5 in summer (a factor of four decrease) (Goericke and Welschmeyer, 1998; Vallina, 2008a). Therefore, the chla-to-carbon ratio we estimate at BBMO is larger than the chla-to-carbon ratio reported at BATS.

4.4. Phytoplankton chla-to-carbon

The values of the chla-to-carbon ratio (mg mg^{-1}) that we observe at the surface in BBMO vary seasonally from ≈0.03 (max) in winter to ≈0.01 (min) in summer (a factor of three decrease) and are twice as large as the seasonal values reported at the surface in BATS, which vary from ≈0.02 (max) in winter to ≈0.005 (min) in summer (a factor of four decrease) (Goericke and Welschmeyer, 1998; Vallina, 2008a). Laboratory estimates of chla-to-carbon in four samples using flow cytometry provide values in the range of 0.004 (min) – 0.015 (max) for phytoplankton species below the 64 μm cell diameter (see Table 3 in Graff et al. (2012)). Nevertheless, the BBMO values are within the range of standard chla-to-carbon conversion (mg mg^{-1}) values reported for marine algae (0.01 to 0.04; see page 185 (Strickland and Parsons, 1972) or 0.02 to 0.05; see Figure 1 in Westberry et al. (2008)). The temporal variability of the chla-to-carbon ratio at BBMO station in Blanes Bay seems to be primarily due to photo-acclimation (Behrenfeld

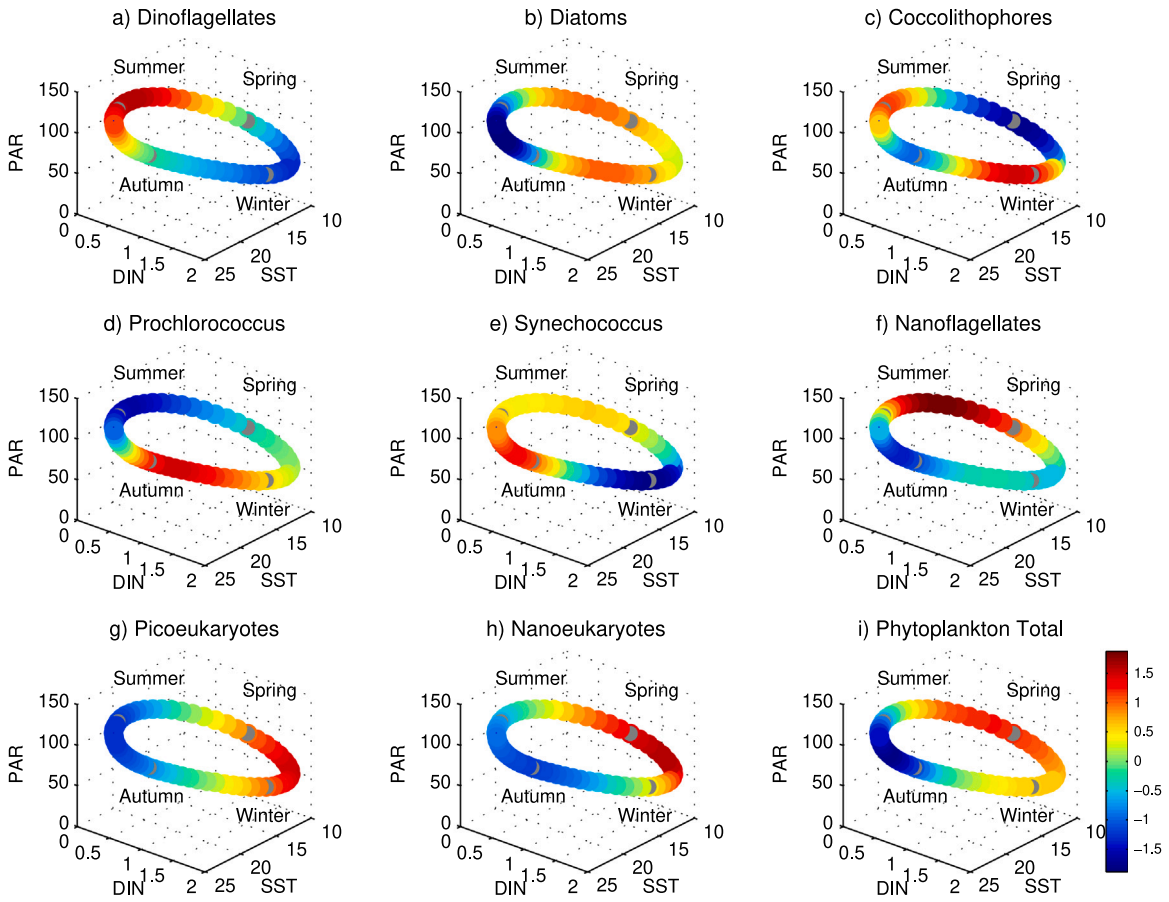

Fig. 17. Niche preferences of each phytoplankton group by plotting their biomass as a function of three major environmental factors: dissolved inorganic nitrogen (DIN), sea surface temperature (SST), and solar irradiance (PAR). Biomass was standardized using the z-score transformation (i.e. subtracting the mean and dividing by the standard deviation) in order to have a standard score value of zero mean and standard deviation equal to one.

et al., 2005; Westberry et al., 2008; Masuda et al., 2021) (see (19) in Box 2), as it is for BATS station in Sargasso Sea and HOT-ALOHA station in Hawaii (Goericke and Welschmeyer, 1998; DuRand et al., 2001; Vallina, 2008a). However, the different annual average of the chla-to-carbon ratio between these time-series can be attributed to their different annual average nutrient level (Cloern et al., 1995) or *nutrient stress* (see Figure 3 in Behrenfeld et al. (2005)). Being BBMO a coastal site in the Blanes Bay, it has a higher nutrient concentration than BATS or HOT-ALOHA stations, which are more oligotrophic systems (Winn et al., 1995; DuRand et al., 2001; Westberry et al., 2008). Therefore a higher synthesis of chla-per-carbon was to be expected in the phytoplankton community of the more eutrophic BBMO, being our chla-to-carbon estimates well within the range of values reported for similar oceanic systems (e.g. 0.01 – 0.03; see region NA-L3 of Figure 2 in Behrenfeld et al. (2005) or see Figure 1j at 40N in Masuda et al. (2021)).

4.5. Phytoplankton growth rate

The phytoplankton growth rate (d^{-1}) that we observe at the surface in BBMO varies seasonally from ≈0.4 in summer to ≈0.8 in winter (a factor of two increase) and are twice as large as the seasonal values reported at the surface in more oligotrophic locations such as BATS, which vary from ≈0.2 to ≈0.4 (Goericke and Welschmeyer, 1998). Yet, our BBMO estimated values are similar to alternative climatological estimates of the phytoplankton growth rate at BATS made with a decade-long time-series of primary production data (≈0.4 in summer and 1.0 in winter; see Figure 1 in Vallina (2008a)) and to growth rates computed at BATS from chlorophyll-specific productivity and carbon-to-chla ratios (Malone et al., 1993). Previous estimates of phytoplankton growth rates at BBMO using dilution experiments are much larger in magnitude than our current estimates and the seasonality is reversed (Gutierrez-Rodriguez et al., 2011). Other estimates of phytoplankton growth rates at BBMO using primary production provide similar values in magnitude to our current estimates, also showing little seasonality (Gasol et al., 2016). The weak seasonality in growth rate is thought to be the result of a strong coupling between biomass-specific production and biomass-specific grazing mortality, with faster growing taxa suffering faster grazing mortality (see Figure 7 in Gutierrez-Rodriguez et al. (2010)).

Given the relatively low seasonality of the climatological signal for our current estimates of phytoplankton growth rate and the high dispersion of the data around the climatological value (see Fig. 6h), we suggest that these estimates should be taken with some caution. The phytoplankton growth rate (d^{-1}) estimates obtained at BBMO during summer (0.4 d^{-1}) are low when compared to the maximum potential growth under temperature-constrain (1.2 d^{-1} for 25 C; see Table 1) (Eppley, 1972), suggesting some degree of nutrient limitation, which is however not too severe probably thanks to the nutrient recycling through ammonium that helps sustaining productivity in summer (see Fig. 5). During the spring bloom the phytoplankton community is close to its maximum value of temperature-constrained growth and therefore the community is probably not nutrient limited. The value of maximum growth rate of 1.2 d^{-1} for the whole phytoplankton community was selected as the mean of the reported maximum growth values for four of the phytoplankton groups (diatoms, 1.8 (d^{-1}); coccolithophores, 1.1

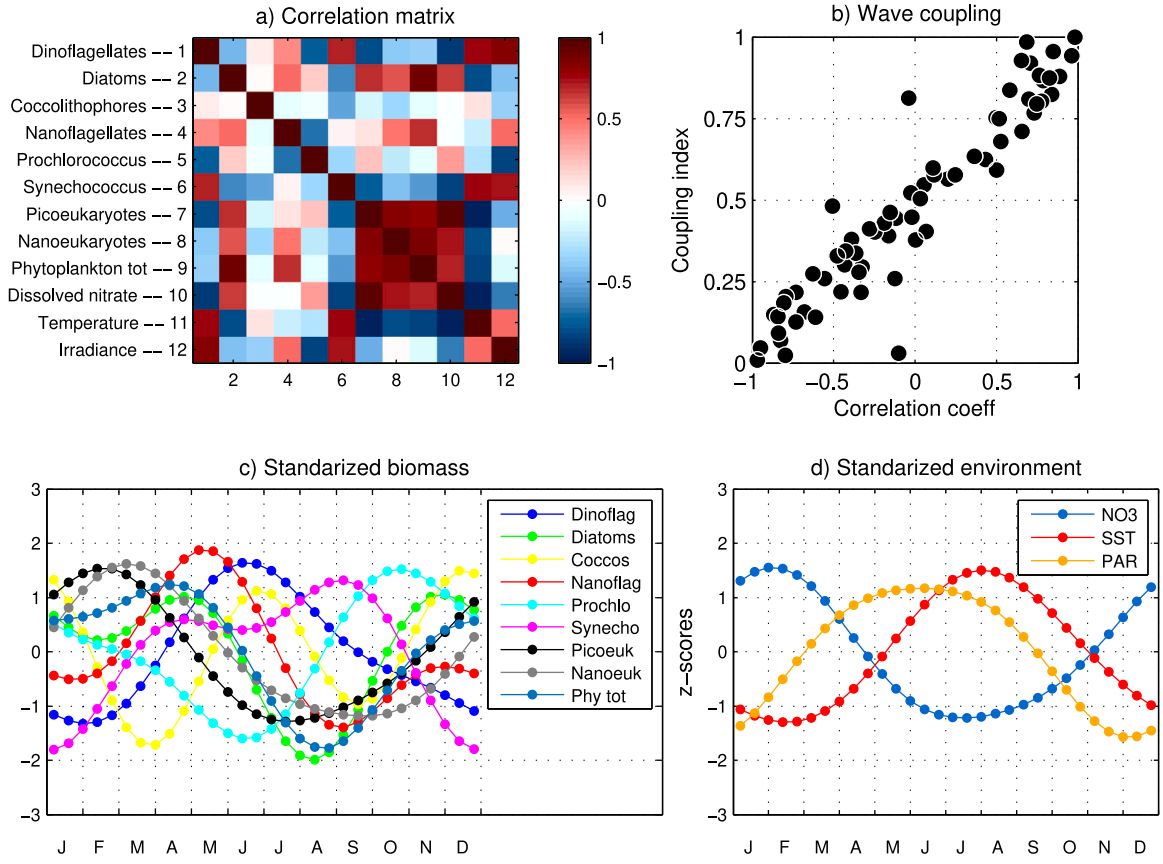

Fig. 18. Seasonal correlation matrix (a) and wave-phase coupling index (b) of selected time-series (c, d). The correlation coefficient and the wave-phase coupling index both provide an estimate of synchrony between pairs of time-series.

(d^{-1}); *Synechococcus*, 1.4 (d^{-1}); *Prochlorococcus*, 0.6 (d^{-1}); see Goericke and Welschmeyer (1998) and references there-in).

4.6. Phytoplankton production

Primary production (mmolC m^{-3} d^{-1}) at BBMO varies seasonally from ≈3.0 in the spring bloom to ≈1.0 in summer (a factor of three decrease). These values are similar to the seasonal values reported at the surface in DYFAMED, which vary from ≈5.0 in the spring bloom to ≈1.0 in summer (a factor of five decrease) (Marty and Chiavérini, 2002). The values in the coastal station BBMO are four times larger than the seasonal values reported at the surface in the open-ocean station BATS, which vary from ≈0.75 in the spring bloom to 0.25 in summer (a factor of three decrease) (Vallina, 2008a). The ecosystem at BBMO thus display an enriched mode during spring that relies on new production (nitrate) and a relatively nutrient-poor mode in summer (not quite oligotrophic) that relies on regenerated production (ammonium). That is, although nutrient supply (and thus nutrient limitation) fluctuates seasonally, the phytoplankton community at BBMO is never severely limited by nutrients. Furthermore, any little imbalance between biomass-specific growth and grazing mortality can have a large effect on phytoplankton biomass and primary production. These two facts may help explain the observation that less than a factor of two seasonal change in specific growth rate (d^{-1}) can lead to a factor of three seasonal change in primary production (mmolC m^{-3} d^{-1}) and to a factor of four seasonal change in phytoplankton biomass (mmolC m^{-3}) (see Figs. 6, 7 and 12)

Primary production at BBMO is positively correlated to chla, carbon biomass and, to a lesser degree, phytoplankton (geometric) mean cell size (see Fig. 15), with Pearson's correlation values between ≈0.3 and 0.4. The correlation value between primary production and carbon biomass (ρ = 0.43) is, however, less strong than the corresponding relationship reported for BATS (ρ = 0.64) (DuRand et al., 2001). The fact that primary production and chla or phytoplankton carbon biomass are well correlated (see Fig. 15a and b) has been already reported for BBMO (Gasol et al., 2016) and across disparate regions of the ocean (Marañón et al., 2014; Cermeño et al., 2016). Yet, the correlation between primary production and chla in the BBMO is significant for autumn through spring, but it is not significant for summer alone (Gasol et al., 2016). Also, the fact that primary production and carbon biomass tend to decrease for smaller mean cell sizes (ρ = 0.30) (see Fig. 15c) was also reported at BATS by showing the (negative) relationship between the relative contribution of pico phytoplankton biomass as a function of primary production (ρ = −0.52) (DuRand et al., 2001). Likewise, a community of phytoplankton dominated by smaller cells has also been associated to lower total carbon biomass in coastal waters of the northwest Iberian peninsula (Marañón, 2015). This scaling between primary production (or carbon biomass) and cell size has been interpreted as a proxy for the biomass-energy flow along the phytoplankton size spectrum, and it has been reported to be actually flat (no significant size-scaling) in the oligotrophic Atlantic Ocean (Huete-Ortega et al., 2012).

4.7. Primary production and growth rate

Direct estimation of primary production and biomass-specific growth rate for different phytoplankton groups is something particularly difficult to obtain. Therefore there is a lack of studies providing seasonal time-series of these two metrics to which compare our estimates shown in Figs. 9 and 10. Yet, the seasonal patterns and the

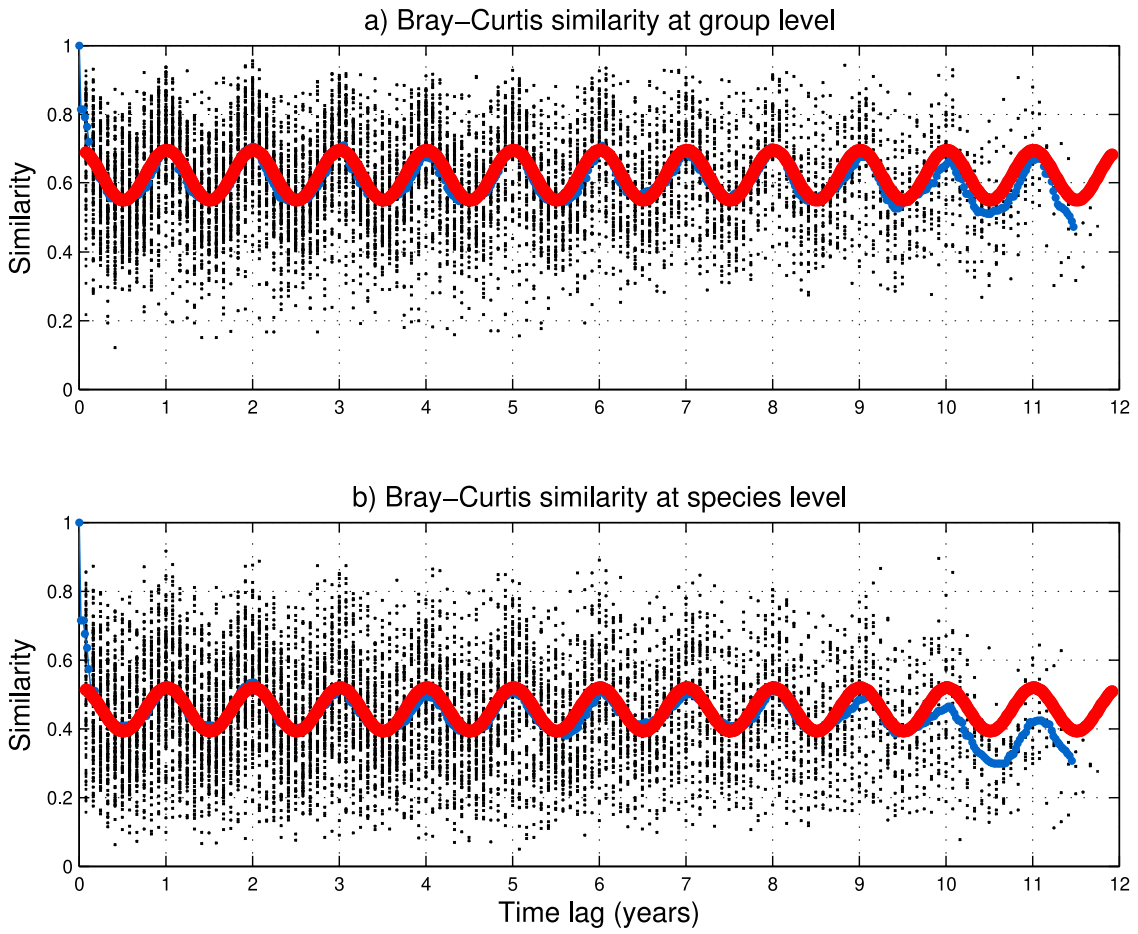

Fig. 19. Bray–Curtis similarity index of phytoplankton community composition as a function of the temporal lag between samples: (a) at the phytoplankton group level, (b) at the phytoplankton species level. The black crosses are the raw data. The blue curve is the averaged data (moving mean). The red curve is a perfect sinusoidal function fitting the data.

absolute values of our estimations for each phytoplankton group are reasonable and agree with the general knowledge we have about some of these groups: diatoms having their fastest growth rate in spring and autumn; *Synechococcus* having it in late summer; picoeukaryotes in winter; nanoeukaryotes in late winter and late summer; dinoflagellates in summer (probably through mixotrophy). These results provide empirical support to earlier theoretical works in ecology regarding the insurance hypothesis of biodiversity (Yachi and Loreau, 1999; Tilman et al., 2001, 2006). Different groups may have distinct ecological niches and respond differently to environmental conditions, leading to an asynchrony in the dynamics of the different groups (Loreau and de Mazancourt, 2013). These asynchronous responses have a buffering or «portfolio effect» on aggregate community-level properties such as total primary production (Yachi and Loreau, 1999). That is, the dynamics of the aggregate properties are stabilized by the presence of several and ecologically diverse array of phytoplankton groups, each of them exploiting best a different ecological niche (Vallina et al., 2017).

4.8. Phytoplankton composition and RAD

The phytoplankton community composition and group dominance changes seasonally (see Figs. 8 and 16). The only two groups that are always rare and thus have very little contribution to total phytoplankton biomass are coccolithophores and *Prochlorococcus*. All other groups show an alternation in dominance at different months of the year. *Prochlorococcus* and *Synechococcus* are seasonally in anti-phase. *Synechococcus* biomass is highest during spring and summer, when *Prochlorococcus* is lowest. *Prochlorococcus* biomass is highest in fall and winter, when *Synechococcus* biomass is lowest. This anti-phase pattern in time between them has been also observed in space (Latasa et al., 2023). Likewise, an opposite seasonal pattern between *Prochlorococcus* and *Synechococcus* have been reported for BATS, although the temporal location of their peaks and valley are not the same as the ones observed for them at BBMO (see Figure 7 in DuRand et al. (2001)). Furthermore, at BATS the depth-integrated biomass of *Prochlorococcus* is much greater than the biomass of *Synechococcus* with the exception of spring (DuRand et al., 2001), while for BBMO it is exactly the opposite situation because *Prochlorococcus* biomass is extremely low and *Synechococcus* biomass is quite high. Indeed, the maximum value of *Prochlorococcus* biomass is (slightly) below the minimum value of *Synechococcus* biomass, and the maximum of *Synechococcus* is one order of magnitude larger than the maximum of *Prochlorococcus* (see Figs. 7 and 16). *Synechococcus* is also known for being present in the upper mixed layer while *Prochlorococcus* tend to occupy deeper depths in the Sargasso Sea (Campbell et al., 1997; DuRand et al., 2001; Casey et al., 2007) and in the NW Mediterranean Sea (Latasa et al., 2022). This may help partially explain the low contribution of *Prochlorococcus* we observe at BBMO, which is located at the very surface of a relatively shallow water column. Furthermore, the BBMO is a coastal site and *Prochlorococcus* are never abundant in coastal temperate sites. This is in part because the light stress is likely too strong for them at the surface of a clear and shallow water column (Sommaruga et al., 2005). Regarding their temporal dynamics at HOT–ALOHA station in Hawaii, *Synechococcus* abundance maxima occur in winter and *Prochlorococcus*

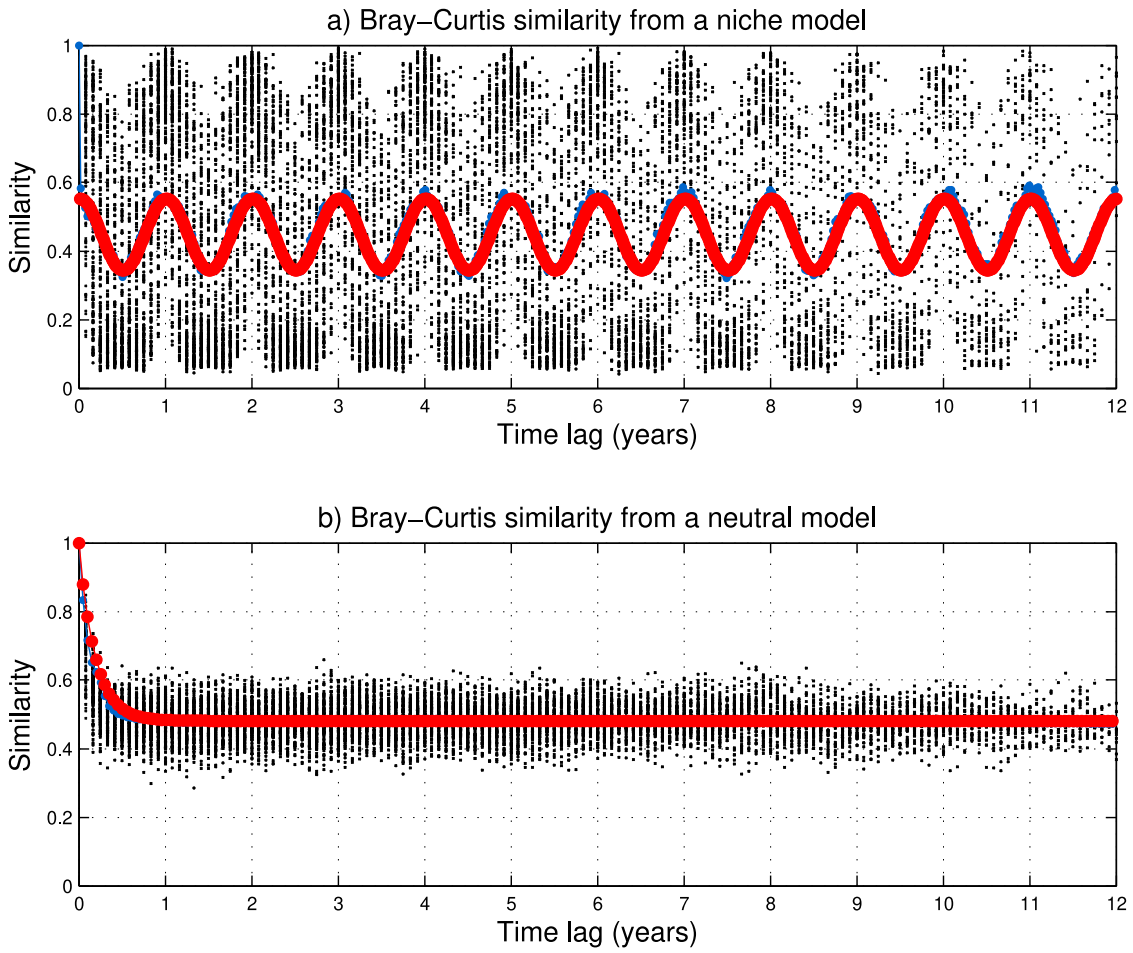

Fig. 20. Bray–Curtis similarity index of a numerically simulated phytoplankton community composition as a function of the temporal lag between samples: (a) for the simulations obtained with the niche model, (b) for the simulations obtained with the neutral model. The black crosses are the raw simulated data. The blue curve is the averaged data (moving mean). The red curve is a perfect function fitting to the data: sinusoidal for the niche model; exponential decay for the neutral model. The numerical simulations were performed using the MIT Darwin model on a chemostat setup.

in summer/fall, quite different timing to the one we observe at BBMO for these two phytoplankton groups. Furthermore, *Prochlorococcus* at ALOHA is always clearly dominant in abundance at all depths (Campbell et al., 1997; van den Engh et al., 2017) and the depth-integrated biomass of *Prochlorococcus* is on average one order of magnitude larger than that of *Synechococcus* (see Figure 8 in Campbell et al. (1997)). This clearly contrasts to our findings at BBMO, where *Synechococcus* biomass always dominates over *Prochlorococcus*. Coccolithophores at BBMO also have an extremely low biomass all year round with a marked minimum in spring (April), while in the Sargasso Sea (i.e. BATS and Hydrostation "S", which are 60 km apart) coccolithophores have been reported to display the greatest abundance in later winter to spring and lowest during summer (DuRand et al., 2001; Haidar and Thierstein, 2001). Our carbon biomass (mmolC m^{-3}) estimates at BBMO of different groups reach maximum values of 0.10 for *Prochlorococcus*; 0.50 for *Synechococcus*; 0.10 for coccolithophores; 1.00 for picoeukaryote phytoplankton; 0.80 for nanoeukaryote phytoplankton; 1.00 for diatoms; and 0.50 for dinoflagellates; (see Fig. 16) For comparison, carbon biomass estimates at BATS of different groups have been reported to reach maximum values of 0.85 for *Prochlorococcus* (eight times higher than in Blanes); 0.50 for *Synechococcus* (similar values to Blanes); 0.30 for coccolithophores (three times higher than in Blanes); and 2.0 for eukaryote phytoplankton, including diatoms (similar values to Blanes if excluding diatoms); Diatoms do not appear to dominate the community at BATS and dinoflagellates were not reported in DuRand et al. (2001). However, other works reported that dinoflagellates (using Peridinin as biomarker) were present at BATS and have a maximum during the summer, yet they were a minor component of the phytoplankton community (Hulburt, 1990; Goericke and Welschmeyer, 1998). By contrast, these two groups dominate the community at BBMO during their seasonal maximum biomass (see Fig. 8).

Previous works using a chemo-taxonomic approach based on HPLC analysis of 28 phytoplankton pigments, in combination with the CHEMTAX algorithm to estimate the contribution of different algal groups to the total chla, have already reported a marked seasonality for total chla and several phytoplankton groups (Nunes et al., 2018). The prasinophytes (green algae such as Micromonas), diatoms, haptophytes (e.g. coccolithophores such as Emiliania huxleyi), cryptophytes (e.g. Cryptomonas) and pelagophytes, were all reported to have an autumn–winter or winter–spring maximum and a summer minimum. This pigment-based approach reported that *Prochlorococcus* have a very low pigment concentration with its maximum in autumn–winter and its minimum in spring–summer; *Synechococcus* have two maxima, one in April and one in August; and dinoflagellates have increased importance during summer. These are exactly the same findings that we report here using an alternative taxonomy-based approach; with the noteworthy exception that the relative contribution of dinoflagellates to total chla in Nunes et al. (2018) is always very low, while the relative contribution to total biomass using our microscopical approach is quite high (even dominant) during summer (compare our Fig. 16 versus Figure 5 in Nunes et al. (2018)). Since dinoflagellates are easily observed under the microscope and all obligate predatory species (no

chla) were removed prior to the analysis, we are confident that our estimates of dinoflagellate seasonality are probably quite accurate. The fact that dinoflagellates dominate in summer suggest that they are doing facultative predatory mixotrophy on small phytoplankton and bacterioplankton to survive during the annual minimum in nutrient concentration. This is supported by the fact that heterotrophic nanoflagellates (HNF zooplankton) that are obligate predators on bacterioplankton show the same seasonal cycle as dinoflagellates (see Figure S2 in Auladell et al. (2019)). The seasonality of diatoms is also very similar for both approaches (compare our Figs. 5 and 7 versus the Figures 6 and 7 in Nunes et al. (2018)). However, the haptophytes group (also called prymnesiophyte in the literature) of Nunes et al. (2018) and our coccolithophores group do not agree, neither in seasonality nor in relative contribution to the total phytoplankton community. The haptophytes in Nunes et al. (2018) is the most dominant group, closely followed by diatoms, while our coccolithophores group is among the least important contributors to total biomass (see Fig. 16). Although coccolithophores make up the majority of haptophyte species, there are other important haptophytes such as *Phaeocystis* that are not coccolithophores. Yet, *Phaeocystis* in particular is not commonly observed at Blanes Bay and therefore there is still some unexplained mismatch between the two approaches regarding these groups.

4.9. Phytoplankton cell size

Fig. 14 (upper left panel) shows an annual climatology of the mean cell size (mean ESD), both in terms of cell abundance and C biomass. Although mean cell size does not change dramatically in absolute values over the annual cycle (≈a factor of two), there is an overall pattern that almost certainly emerges from differences in water column hydrodynamics. This pattern is particularly obvious for the annual climatology of mean cell size constructed from cell abundance estimates, which reflects the seasonal succession of phytoplankton groups, from large diatoms to autotrophic picoplankton, as summer progresses and water column stratification intensifies. Cell size is a master trait that governs many ecophysiological features of phytoplankton, including their light absorption efficiencies, nutrient uptake and metabolic rates (Finkel et al., 2010; Cermeño et al., 2006; Marañón, 2015; Hillebrand et al., 2021). As cell sizes increases, the surface to volume ratio decreases. Because light and nutrients enter the cells through their surface, a decrease in the surface area to volume ratio inevitably leads to a reduction in the photosynthetic efficiency of the cells (Kiorboe, 1993; Raven, 1998). Phytoplankton size structure also determines the fate of the recently photosynthesized organic matter, which is either recycled or exported depending on whether phytoplankton communities are dominated by small or large-sized species, respectively (Legendre and Fevre, 1995). Typically, communities dominated by small-sized, picoplankton species, such as *Prochlorococcus*, are characteristic of stratified ecosystems where the main source of inorganic nutrients is in-situ remineralization of organic matter. In contrast, communities dominated by large-sized species, such as diatoms, are characteristic of unstable ecosystems where river runoff, atmospheric deposition and/or upwelling of nutrient-rich deep waters fertilize the surface waters. This is consistent with the observation that the mean cell sizes during winter double with respect to those of summer, when reduced river discharges and water column stratification limit external nutrient supplies. We attribute the observation that size diversity peaks at intermediate levels of mean cell size (see Fig. 14, lower left panel) to the fact that the number of species in both extremes (small and large cell sizes) is smaller than at intermediate cell sizes, leading to a consistent and statistically significant decrease in variance (size diversity). This explanation is also consistent with the observation that size diversity (ESD sigma) increased in concert with the exp Shannon index for species diversity.

4.10. Phytoplankton ecological niches

Dinoflagellates at the BBMO are very abundant and have a clear annual maximum in summer (see Figs. 7 and 17). In fact they can dominate the total phytoplankton biomass (June, July, August; see Figs. 8 and 16). This agrees with the environmental niche of dinoflagellates at BATS which is located in summer-time conditions (Goericke and Welschmeyer, 1998). Summer is the season with lowest nutrient availability but dinoflagellates in the BBMO display a seasonal maximum that is one order of magnitude higher than their winter-time minimum, which suggest that mixotrophic (predatory) grazing can be a source of nutrients for dinoflagellates (Unrein et al., 2007; García-Oliva et al., 2022). Note that all dinoflagellate species without chla content were discarded from the analysis to exclude obligate predatory species. Yet, facultative predatory mixotrophy on small phytoplankton and bacterioplankton is a well known source of food intake for many dinoflagellate species to supplement their diet under limited photosynthetic conditions (Unrein et al., 2007; Ward and Follows, 2016). Although coccolithophores in the BBMO are never abundant, they have an annual maximum in winter. The winter-time conditions at BBMO agree well to the environmental conditions where the dominant coccolithophore (*Emiliania huxleyi*) at Hydrostation "S" in the Sargasso Sea has been reported to grow best, which are low temperature (≈20 C) and low-to-moderate PAR (>3.0 W m^{-2}) (see Figure 11 in Haidar and Thierstein (2001)). Nutrients are always quite low in the surface layers at Hydrostation "S" (<0.7 mmolN m^{-3} of nitrate concentration) when compared to Blanes Bay (<2.0 mmolN m^{-3} of nitrate concentration). Diatoms typically monopolize nutrients during spring mixing of the water column and subsequent nutrient injection, leading to the formation of spring diatom blooms. Nutrient depletion during prolonged periods of stratification benefits other groups of phytoplankton, which are superior competitors under conditions of nutrient scarcity. The Margalef Mandala shows that diatoms are succeeded by dinoflagellates during summer stratification. However, other groups such as *Synechococcus*, picoeukaryotes, or photosynthetic nanoflagellates can also thrive under these conditions due to their high affinity for nutrients, which implies they have high ability to take up nutrients at relatively low concentrations.

4.11. Phytoplankton α-diversity and β-diversity

Fig. 8(i) provides an estimate of the seasonality of α-diversity, a measure of local *effective richness* of phytoplankton groups. The climatological values oscillate between 0.6 units in winter and 0.8 units summer (1.33 fold change from valley to peak), being the units the fraction to its maximum potential richness (eight phytoplankton groups). Despite this seasonal cycle, α-diversity is high throughout the year: more than half the phytoplankton groups are effectively present in the community, and then having a contribution to ecosystem functioning. The fact that α-diversity is lowest during winter and highest during summer in temperate ecosystems has been suggested before to be the result of a stronger competitive exclusion in winter than in summer, due to the dominance of fast-growing opportunistic phytoplankton groups (such as diatoms) during the seasonal upwelling by vertical turbulence that brings nutrients to the surface in winter (Vallina et al., 2014a).

Fig. 19 provides an estimate of β-diversity in time, a measure of compositional heterogeneity and phytoplankton group or phytoplankton species turnover. The raw data values oscillate between 0.2 and 0.8 units of similarity, while the averaged data (moving mean) and the sinusoidal fitting curve oscillate roughly between 0.4 and 0.6 units. The similarity index is consistently ≈0.2 units larger at the group level than at the species level. There is an obvious repeated cycle in the similarity index with a periodicity of one year, which was to be expected given the repeated seasonal patterns observed for the phytoplankton groups at the Blanes Bay time-series. The same oscillatory nature of β-diversity has been shown for the taxonomic groups (using 18S rRNA gene data)

constituting the picoeukaryotic and nanoeukaryotic communities in the BBMO (Giner et al., 2019), for several functional groups (defined by a marker gene) of photosynthetic bacteria in the BBMO (Auladell et al., 2019), and for marine bacterial communities at the L4 Ocean Observatory time-series of the English Channel (Hatosy et al., 2013).

This pattern for prokaryotes was first observed by Fuhrman et al. (2006, 2015) and it has been shown for both eukaryotes and prokaryotes at BBMO not just for the pufM gene (Krabberod et al., 2022), which codes for an essential protein of the photo-system II (the core of the photosynthetic reaction center) common to all bacteria with a type-II photosynthetic apparatus. What is remarkable in our study is that we obtain the same sinusoidal pattern with much less species or phytoplankton groups than in these other studies using 16S or 18S rRNA gene diversity. This suggests that this pattern is very robust. The fact that a perfect sinusoidal function is able to fit the β-diversity in time at BBMO, implies that this ecosystem is most probably following niche dynamics instead of neutral dynamics that predicts an exponential decay of community similarity with spatiotemporal distance (Nekola and White, 1999; Fuhrman et al., 2015; Villarino et al., 2018).

The results of temporal β-diversity obtained from the observational data at BBMO are similar to the theoretical prediction obtained by the niche model simulation (see Figs. 19 and 20). By contrast, the prediction obtained by the neutral model simulation fails to explain the observed patterns. While the niche theory simulation correctly predicts a sinusoidal behavior of temporal β-diversity, the neutral theory simulation predicts an exponential decay that is not observed in the data. To the best of our knowledge, this is the first time that the shape of β-diversity as a function of the temporal distance (time-lag) between samples has been formally simulated using a mechanistic modeling approach. Phytoplankton group replacement or temporal turnover, defined as (1 - β-diversity) at time-lag of one month (Righetti et al., 2019), happens faster in spring and autumn than during the rest of the year, the first pulse increases α-diversity and the second pulse decreases it (see Fig. 8i). The two cycles per year (six-month periodicity) observed at BBMO for phytoplankton group turnover vary a factor of two from valley (20%) to peak (40%). These two peaks are suggestive of a causal relationship with water column stratification dynamics: the first annual peak of turnover is coincident with the late spring (April) thermal stratification of the water column, while the second annual peak is coincident with the late autumn (October) breaking of the summer-time thermal stratification. That is, the two annual peaks of temporal turnover are in synchrony with the two major change events in water column mixing dynamics (see Fig. 3d). When water column structure is constant, such as in winter (homogeneous, well mixed vertically) and in summer (stratified, strong gradient vertically), the phytoplankton group turnover is minimum (see Figs. 8i and 3d).

5. Conclusion

This work provides a detailed description of the phytoplankton community at BBMO using ten years of monthly sampling with corresponding environmental conditions, in order to better understand the mechanisms that dictate the seasonal dynamics of the major phytoplankton groups and explain the observed shifts in community structure. The main goal was to help answering the following question: does the temporal community assembly of marine phytoplankton follow the mechanisms defined by the niche-theory or the neutral-theory? Using empirical data, we assessed the validity of these two competing theoretical explanations of the rules of community assembly in marine phytoplankton. With that aim, we perform an in-depth analysis of the seasonal patterns for the eight major phytoplankton groups observed at Blanes Bay: dinoflagellates, diatoms, coccolithophores, *Prochlorococcus*, *Synechococcus*, picoeukaryotes, and nanoeukaryotes. The BBMO time-series is one of the largest data sets resolving phytoplankton species composition available, along with the synoptic conditions of their local environment: nutrients, temperature, irradiance.

We provide information on the phytoplankton α-diversity (or local *effective richness*) using the exponential of the Shannon index; the temporal β-diversity (or one minus the *species-turnover*) using the Bray–Curtis similarity index of community composition, both at the species-level and at the group-level; the diversity of cell sizes; the phytoplankton biomass, primary production, and growth rate; estimates of the regenerated production; estimates of the chla-to-carbon ratio; monthly rank-abundance (here rank-biomass) distributions of phytoplankton groups; the environmental niche characterization of the phytoplankton groups (i.e. the relationship between the seasonality of phytoplankton groups and the environmental variables such as nutrient concentration, water temperature and solar irradiance); among other analyses. These large set of detailed and in-depth analyses provide empirical support to the niche theory for marine phytoplankton ecology and community assembly. This result is important from the point of predicting and understanding phytoplankton community dynamics using either mechanistic models (i.e. numerical models) or species distribution models (i.e. niche models) that are deeply rooted on the notion that the target species or groups of interest have fundamental niches (*sensu* Hutchinson (Hutchinson, 1957, 1961)) related to the environmental conditions, and therefore that their biogeography is in theory predictable.

Therefore, the climatological time-series presented here can serve as an excellent testing ground for evaluating the performance of marine ecosystem models having an explicit representation of different phytoplankton groups. The climatological data presented here can be downloaded as open access (https://www.oceanglobe.info/MAT/) and loaded using the free open-source software **GNU Octave** (https://octave.org/). The development of ocean ecosystem models is still strongly hampered by the paucity of good time-series longer than a few years. An additional decade of observations may also allow us to discern in future research some of the major modes of interannual variability at the BBMO site, such as the El Niño-Southern Oscillation (ENSO) or the North Atlantic Oscillation (NAO). Currently, the structure of the interannual variability at BBMO remains largely unknown given the muted (low amplitude) annual cycles relative to seasonal cycles at BBMO, probably due to the still rather short duration of the time-series from the point of view of studying interannual dynamics.

Declaration of competing interest

The authors declare that they have no known competing financial interests or personal relationships that could have appeared to influence the work reported in this paper.

Data availability

Data will be made available on request

Acknowledgments

This work was funded by national research grant MARES (CGL2013-41256-P) from the Spanish government to S.M.V. Data were collected and processed by several grants from the Spanish government and the European Union. The Blanes Bay Microbial Observatory (BBMO) has been operating since 1992 as an observatory of the coastal pelagic ecosystem of the NW Mediterranean. We would like to thank all the people involved with maintaining the BBMO time-series and particularly R. Massana, C. Cardelús, V. Balagué, J.M.G. and C.M. for coordination of the series, sampling, and basic data processing. C.G. was supported by a PhD fellowship grant within the MARES project. The Institute of Marine Sciences (CSIC) received funding from the

Spanish government through the «Severo Ochoa Centre of Excellence» award (CEX2019-000928-S). All authors contributed to and reviewed the manuscript. We would like to thank Prof. Hugh Ducklow and an anonymous reviewer for their comments and suggestions to improve this article during the peer-review process.

Appendix

The NPZD multi-species model resolves 64 phytoplankton ecotypes, a generic zooplankton ecotype, a generic detritus pool, and a single elemental nutrient (nitrogen). Only detritus is subject to a sinking loss term. The model resolves two trophic levels: photo-autotrophic phytoplankton, and herbivorous zooplankton. The generic herbivore zooplankton feeds upon all phytoplankton ecotypes following a killing-the-winner (KTW) predation strategy (Vallina et al., 2014b). While carnivorous zooplankton is not explicitly modeled, its top-down control on herbivorous zooplankton is implicitly simulated using a quadratic predatory mortality acting as a closure term (Eq. (38)). The recycling of nutrients assumes linear constant degradation rates of detritus. The rate of change of the simulated phytoplankton (Eq. (23)) and zooplankton (Eq. (24)) results from the balance between gross production (Eqs. (27) and (28)), exudation due to respiration (Eqs. (36) and (37)), constant mortality (Eqs. (34) and (35)), and the mechanical losses by chemostat dilution (overflow) rate (Eq. (45)). Phytoplankton production (Eq. (27)) is a function of nutrient limitation (Eq. (29)), irradiance limitation (Eq. (30)), and temperature limitation (Eq. (31)). The functional responses for these "nutrient–irradiance–temperature" limitations, are assumed to be different among the phytoplankton ecotypes when simulating the niche-dynamics community (Follows et al., 2007; Vallina et al., 2017), while they are assumed to be equal for all phytoplankton ecotypes when simulating the neutral-dynamics community (Vallina et al., 2017). The model was run for 12 years using as environmental forcing (solar irradiance, sea temperature) the observations at BBMO. Nutrient concentration was not imposed because it is a state-variable of the model. We imposed a sinusoidal supply of nutrients instead (see Eq. (41)). The model parameters are given in Table 2.

The model uses a chemostat-bioreactor setup that allows for controlling the immigration and emigration processes of any of the state variables. In particular, we place the focus on phytoplankton inflow to the local community from an external regional pool (immigration) and on phytoplankton outflow from the local community (emigration). The external regional pool is assumed to have a constant (invariant) and homogeneous (flat) distribution of the 64 phytoplankton ecotypes. Under the simulated niche-dynamics scenario, the immigration and emigration rate is constant an affects equally all phytoplankton ecotypes; that means, the dilution rate of the chemostat dictates the inflow and outflow concentration of phytoplankton ecotypes in a deterministic fashion without any stochasticity (without any randomness) associated to it. Under the simulated neutral-dynamics scenario, the immigration and emigration are different for each phytoplankton ecotype by means of assuming that inflow to and outflow from the chemostat are subject to a binary stochastic processes (0,1) at a weekly frequency that multiplies the background dilution rate. This approach leads to two contrasting scenarios: (i) under the niche-dynamics, the local assembly of the phytoplankton community is governed by ecological trait and fitness differences among the ecotypes (MacArthur, 1968), being the immigration and emigration equal for all ecotypes; (ii) under the neutral-dynamics, the local assembly of the phytoplankton community is governed by stochastic immigration and emigration processes (Hubbell, 2001, 2005), being the ecological trait values and fitness equal for all ecotypes (Vallina et al., 2017). In the niche-dynamics simulation, there are four different nutrient concentration optima (N_{opt}), four different solar irradiance optima (I_{opt}), and four different temperature optima (T_{opt}); which leads to $4 \times 4 \times 4 = 64$ phytoplankton ecotypes with different ecological traits. In the neutral-dynamics simulation, there is only one N_{opt}, one I_{opt}, and one T_{opt}; which leads to 64 phytoplankton ecotypes that are ecologically equivalent and thus competitively neutral (Vallina et al., 2017). Note that N_{opt} is directly related to μ_j and equal to the half-saturation constant for nutrient uptake K_{P_j} (see Vallina et al. (2017) for mathematical details).

Box 3 | NPZD niche–neutral model

$$\frac{\partial P_i}{\partial t} = \overbrace{F_{P_i} - E_{P_i} - G_{P_i} - M_{P_i}}^{\text{Biological terms}} \overbrace{+ \phi_i(t)\,\lambda\,P_i^{ref}}^{\text{Immigration}} \overbrace{- \varphi_i(t)\,\lambda\,P_i}^{\text{Emigration}} \quad (23)$$

$$\frac{\partial Z}{\partial t} = F_Z - E_Z - G_Z - M_Z + \lambda\,(Z^{ref} - Z) \quad (24)$$

$$\frac{\partial N}{\partial t} = S_N + \lambda\,(N^{ref} - N) - F_P \quad (25)$$

$$\frac{\partial D}{\partial t} = S_D + \lambda\,D - \omega\,D \quad (26)$$

$$F_P = \sum_i F_{P_i} = \sum_i (\gamma_i^N\,\gamma_i^I\,\gamma_i^T)\,\mu_i P_i \quad (27)$$

$$F_Z = \sum_i G_{P_i} = \sum_i \frac{P_i^{\alpha_Z}}{(\sum_k P_k^{\alpha_Z})}\,\frac{\sum_k P_k}{K_Z + \sum_k P_k}\,(\mu_z\,Z) \quad (28)$$

$$\gamma_i^N = \frac{N}{K_{P_i} + N} \quad (29)$$

$$\gamma_i^I = \frac{I}{I_i^{sat}}\,\exp\left(1 - \frac{I}{I_i^{sat}}\right) \quad (30)$$

$$\gamma_i^T = \exp\left(\frac{T - T_i^{opt}}{\sigma_T}\right)\left(\frac{T_i^{opt} - T + \sigma_T}{\sigma_T}\right)\,\text{Eppley} \quad (31)$$

$$\text{Eppley} = \exp(\alpha_T\,(T_i^{opt} - T_{max})) \quad (32)$$

$$\alpha_T = \log(Q_{10})/10 \quad (33)$$

$$M_P = m_p \sum_i P_i \quad (34)$$

$$M_Z = m_z\,Z \quad (35)$$

$$E_P = (1 - \beta_P)\,F_P \quad (36)$$

$$E_Z = (1 - \beta_Z)\,F_Z \quad (37)$$

$$G_Z = (m_z / Z^{ref})\,Z^2 \quad (38)$$

$$S_N = \varepsilon\,(E_P + E_Z + M_P + M_Z + G_Z) + m_d\,PON \quad (39)$$

$$S_D = (1 - \varepsilon)\,(E_P + E_Z + M_P + M_Z + G_Z) - m_d\,PON \quad (40)$$

$$N^{ref} = N_{min} + ((N_{max} - N_{min})/2)\,(1 + \sin(\Omega\,(t - \tau))) \quad (41)$$

$$P_i^{ref} = P_{ref} \,/\, \text{nphy} = \text{constant} \quad (42)$$

$$\Omega = (2\,\pi) \,/\, \text{T} \quad (43)$$

$$\tau = (3/4)\,\text{T} \quad (44)$$

$$\lambda = 0.1(\text{d}^{-1}) \quad (45)$$

$$\phi_i(t) = [0, 1]\ \text{binary random integer (weekly frequency)} \quad (46)$$

$$\varphi_i(t) = [0, 1]\ \text{binary random integer (weekly frequency)} \quad (47)$$

Table 2
NPZD niche–neutral model parameters.

Parameter		Sym	Value	Units
Phy	max uptake rate	μ_j	0.5–4	d^{-1}
Phy	Halfsat for uptake	K_{P_j}	0.05–2	mmolN m^{-3}
Phy	Optimal temperature	T_i^{opt}	12–24	°C
Phy	Optimal irradiance	I_i^{sat}	20–160	W m^{-2}
Phy	Temperature tolerance	σ_T	4	°C
Phy	Assimilation efficiency	β_P	1/3	n.d.
Phy	Excretion to nutrients	ϵ	1/3	n.d.
Phy	Mortality rate	m_p	0.05	d^{-1}
Phy	External concentration	P_{ref}	0.5	mmolN m^{-3}
Phy	Species richness max	nphy	64	#
Zoo	max grazing rate	μ_Z	2	d^{-1}
Zoo	Halfsat for grazing	K_Z	0.5	mmolN m^{-3}
Zoo	Kill-the-winner param	α_Z	1.8	n.d.
Zoo	Assimilation efficiency	β_Z	2/3	n.d.
Zoo	Excretion to nutrients	ϵ	1/3	n.d.
Zoo	Mortality rate	m_z	0.05	d^{-1}
Zoo	External concentration	Z_{ref}	0.5	mmolN m^{-3}
Nut	min nutrient ext conc	N_{min}	0.1	d^{-1}
Nut	max nutrient ext conc	N_{max}	1.0	d^{-1}
Det	Degradation rate	m_d	0.1	d^{-1}
Det	Sinking rate	ω	0.5	m d^{-1}

References

Acevedo-Trejos, E., Gunnar, B., Bruggeman, J., Merico, A., 2015. Mechanisms shaping size structure and functional diversity of phytoplankton communities in the ocean. Sci. Rep. 5, 8918. http://dx.doi.org/10.1038/srep08918.

Ahumada-Sempoal, M.A., Flexas, M.M., Bernardello, R., Bahamon, N., Cruzado, A., Reyes-Hernandez, C., 2015. Shelf-slope exchanges and particle dispersion in blanes submarine canyon (nw mediterranean sea): A numerical study. Cont. Shelf Res. 109, 35–45. http://dx.doi.org/10.1016/j.csr.2015.09.0120278-4343/.

Aubry, F.B., Berton, A., Bastianini, M., Socal, G., Acri, F., 2004. Phytoplankton succession in a coastal area of the NW Adriatic, over a 10-year sampling period (1990–1999). Cont. Shelf Res. 24, 97–115.

Auladell, A., Sanchez, P., Sanchez, O., Gasol, J.M., Ferrera, I., 2019. Long-term seasonal and interannual variability of marine aerobic anoxygenic photoheterotrophic bacteria. ISME J. 13, 1975–1987. http://dx.doi.org/10.1038/s41396-019-0401-4.

Bahamon, N., Aguzzi, J., Ahumada-Sempoal, M.A., Bernardello, R., Reuschel, C., Company, J.B., Peters, F., Gordoa, A., Navarro, J., Velásquez, Z., Cruzado, A., 2020. Stepped coastal water warming revealed by multiparametric monitoring at nw mediterranean fixed stations. MDPI Sens. 20 (2658), http://dx.doi.org/10.3390/s20092658.

Bahamon, N., Aguzzi, J., Bernardello, R., …, Cruzado, A., 2011. The new pelagic operational observatory of the catalan sea (oocs) for the multisensor coordinated measurement of atmospheric and oceanographic conditions. MDPI Sens. 11 (12), 11251–11272. http://dx.doi.org/10.3390/s111211251.

Behrenfeld, M.J., Boss, E., Siegel, D.A., Shea, D.M., 2005. Carbon-based ocean productivity and phytoplankton physiology from space. Glob. Biogeochem. Cycles 19 (GB1006), http://dx.doi.org/10.1029/2004GB002299.

Bernardello, R., Cardoso, J., Bahamon, N., Donis, D., Marinov, I., Cruzado, A., 2012. Factors controlling interannual variability of vertical organic matter export and phytoplankton bloom dynamics – a numerical case-study for the NW Mediterranean Sea. Biogeosciences 9, 4233–4245.

Bloomfield, P., 2000. Fourier Analysis of Time Series: An Introduction. In: Wiley Series in Probability and Statistics, John Wiley & Sons, New York.

Brock, T.D., 1981. Calculating solar radiation for ecological studies. Ecol. Model. 14, 1–19.

Cadotte, M., 2017. Functional traits explain ecosystem function through opposing mechanisms. Ecol. Lett..

Campbell, L., Liu, H., Nolla, H.A., Vaulot, D., 1997. Annual variability of phytoplankton and bacteria in the subtropical north pacific ocean at station aloha during the 1991–1994 enso event. Deep Sea Res. I 44 (2), 167–192. http://dx.doi.org/10.1016/S0967-0637(96)00102-1.

Casey, J.R., Lomas, M.W., Mandecki, J., Walker, D.E., 2007. Prochlorococcus contributes to new production in the sargasso sea deep chlorophyll maximum. Geophys. Res. Lett. 34, http://dx.doi.org/10.1029/2006GL028725.

Cermeño, P., Choucino, P., Fernandez-Castro, B., Figueiras, F.G., Maranon, E., Marrase, C., Mourino-Carballido, B., Perez-Lorenzo, M., Rodriguez-Ramos, T., Teixeira, I.G., Vallina, S.M., 2016. Marine primary productivity is driven by a selection effect. Front. Mar. Sci. 3, http://dx.doi.org/10.3389/fmars.2016.00173.

Cermeño, P., Marañón, E., Harbour, D., Harris, R.P., 2006. Invariant scaling of phytoplankton abundance and cell size in contrasting marine environments. Ecol. Lett. 9 (11), 1210–1215. http://dx.doi.org/10.1111/j.1461-0248.2006.00973.x.

Charles, F., Lantoine, F., Brugel, S., Chretiennot-Dinet, M.-J., Riviere, B., 2005. Seasonal survey of the phytoplankton biomass, composition and production in a littoral NW Mediterranean site, with special emphasis on the picoplanktonic contribution. Estuar. Coast. Shelf Sci. 65 (1–2), 199–2012.

Chatfield, C., 2004. The Analysis of Time Series: An Introduction. CRC Press, Chapman and Hall, Boca Raton.

Chust, G., Irigoien, X., Chave, J., Harris, R., 2012. Latitudinal phytoplankton distribution and the neutral theory of biodiversity. Global Ecol. Biogeogr. 22 (5682).

Claustre, H., Legendre, L., Boyd, P.W., Levy, M., 2021. The oceans' biological carbon pumps: Framework for a research observational community approach. Front. Mar. Sci. 8, http://dx.doi.org/10.3389/fmars.2021.780052.

Cloern, J.E., Grenz, C., Vidergar-Lucas, L., 1995. An empirical model of the phytoplankton chlorophyll: carbon ratio-the conversion factor between productivity and growth rate. Limnol. Oceanogr. 40 (7), 1313–1321. http://dx.doi.org/10.4319/lo.1995.40.7.1313.

Cropp, R.A., Norbury, J., Gabric, A.J., Braddock, R.D., 2004. Modeling dimethylsulphide production in the upper ocean. Glob. Biogeochem. Cycles 18, http://dx.doi.org/10.1029/2003GB002126.

D'Ortenzio, F., d'Alcala, M.R., 2009. On the trophic regimes of the mediterranean sea: a satellite analysis. Biogeosciences 6 (2), 139–148. http://dx.doi.org/10.5194/bg-6-139-2009.

DuRand, M.D., Green, R.E., Sosik, H.M., Olson, R.J., 2002. Diel variations in optical properties of micromonas pusill (pramsinophyceae). J. Phycol. 38 (6), 1132–1142. http://dx.doi.org/10.1046/j.1529-8817.2002.02008.x.

DuRand, M.D., Olson, R.J., Chisholm, S.W., 2001. Phytoplankton population dynamics at the bermuda atlantic time-series station in the sargasso sea. Deep-Sea Res. II 48, 1983–2003.

Dutkiewicz, S., Cermeño, P., Jahn, O., Follows, M.J., Hickman, A.E., T, D.A.A., Ward, B.A., 2020. Dimensions of marine phytoplankton diversity. Biogeosciences 17, 609–634. http://dx.doi.org/10.5194/bg-17-609-2020.

Eppley, R.W., 1972. Temperature and phytoplankton growth in the sea. Fish. Bull. 70 (4), 1063–1085.

Eppley, R.W., Peterson, B.J., 1979. Particulate organic matter flux and planktonic new production in the deep ocean. Nature 282 (5740), 677–680. http://dx.doi.org/10.1038/282677a0.

Estrada, M., Latasa, M., Emelianov, M., Gutierrez-Rodriguez, A., Fernandez-Castro, B., Isern-Fontanet, J., Mourino-Carballido, B., Salat, J., Vidal, M., 2014. Seasonal and mesoscale variability of primary production in the deep winter-mixing region of the NW Mediterranean. Deep Sea Res. I 194, 45–61.

Faith, D.P., Minchin, P., Belbin, L., 1987. Compositional dissimilarity as a robust measure of ecological distance. Vegetatio 69, 57–68. http://dx.doi.org/10.1007/BF00038687.

Falkowski, P.G., Barber, R.T., Smetacek, V., 1998. Biogeochemical controls and feedbacks on ocean primary production. Science 281 (5374), 200–206. http://dx.doi.org/10.1126/science.281.5374.200.

Field, C.B., Behrenfeld, M.J., Randerson, J.T., Falkowski, P., 1998. Primary production of the biosphere: Integrating terrestrial and oceanic components. Science 281, 237–240. http://dx.doi.org/10.1126/science.281.5374.237.

Finkel, Z.V., Beardall, J., Flynn, K.J., Quigg, A., Rees, T.A.V., Raven, J.A., 2010. Phytoplankton in a changing world: cell size and elemental stoichiometry.

Follows, M.J., Dutkiewicz, S., 2011. Modeling diverse communities of marine microbes. Annu. Rev. Mar. Sci. 3, 427–451.

Follows, M.J., Dutkiewicz, S., Grant, S., Chisholm, S.W., 2007. Emergent biogeography of microbial communities in a model ocean. Science 315, 1843–1846.

Fuhrman, J.A., Cram, J.A., Needham, D.M., 2015. Marine microbial community dynamics and their ecological interpretation. Nat. Rev. Microbiol. 13 (3), 133–146.

Fuhrman, J.A., Hewson, I., Schwalbach, M.S., Steele, J.A., Brown, M.V., Naeem, S., 2006. Annually reoccurring bacterial communities are predictable from ocean conditions. Proc. Natl. Acad. Sci. 103 (35), 13104–13109. http://dx.doi.org/10.1073/pnas.0602399103.

García-Oliva, O., Hantzsche, F.M., Boersma, M., Wirtz, K.W., 2022. Phytoplankton and particle size spectra indicate intense mixotrophic dinoflagellates grazing from summer to winter. J. Plankton Res. http://dx.doi.org/10.1093/plankt/fbac013.

Gasol, J.M., Cardelús, C., Morán, X.A.G., Balagué, V., Forn, I., Marrasé, C., Massana, R., Pedrós-Alió, C., Sala, M.M., Simó, R., Vaqué, D., Estrada, M., 2016. Seasonal patterns in phytoplankton photosynthetic parameters and primary production at a coastal nw mediterranean site. Sci. Mar. 80S1, http://dx.doi.org/10.3989/scimar.04480.06E.

Giner, C.R., Balagué, V., Krabberød, A.K., Ferrera, I., Reñé, A., Garcés, E., Gasol, J.M., Logares, R., Massana, R., 2019. Quantifying long-term recurrence in planktonic microbial eukaryotes. Mol. Ecol. 28 (5), 923–935. http://dx.doi.org/10.1111/mec.14929.

Goericke, R., Welschmeyer, N.A., 1998. Response of sargasso sea phytoplankton biomass, growth rates and primary production to seasonally varying physical forcing. J. Plankton Res. 20 (12), 2223–2249.

Graff, J.R., Milligan, A.J., Behrenfeld, M.J., 2012. The measurement of phytoplankton biomass using flow-cytometric sorting and elemental analysis of carbon. Limnol. Oceanogr.: Methods 10 (11), 910–920. http://dx.doi.org/10.4319/lom.2012.10.910.

Guadayol, O., Peters, F., Marrase, C., Gasol, J.M., Roldan, C., Berdalet, E., Massana, R., Sabata, A., 2009. Episodic meteorological and nutrient-load events as drivers of coastal planktonic ecosystem dynamics: a time-series analysis. Mar. Ecol. Prog. Ser. 381, 139–155.

Gutierrez-Rodriguez, A., Latasa, M., Estrada, M., Vidal, M., Marrase, C., 2010. Carbon fluxes through major phytoplankton groups during the spring bloom and post-bloom in the northwestern mediterranean sea. Deep-Sea Res. I 57, 486–500.

Gutierrez-Rodriguez, A., Latasa, M., Scharek, R., Massana, R., Vila, G., Gasol, J.M., 2011. Growth and grazing rate dynamics of major phytoplankton groups in an oligotrophic coastal site. Estuar. Coast. Shelf Sci. 95, 77–87.

Haidar, A.T., Thierstein, H.R., 2001. Coccolithophore dynamics off bermuda (n. atlantic). Deep-Sea Res. 48, 1925–1956.

Hansen, H., Koroleff, F., 1999. Determination of dissolved inorganic phosphate. In: Method of Seawater Analysis.

Hatosy, S.M., Martiny, J.B.H., Sachdeva, R., Steele, J., Fuhrman, J.A., Martiny, A.C., 2013. Beta diversity of marine bacteria depends on temporal scale. Ecology 94 (9), 1898–1904. http://dx.doi.org/10.1890/12-2125.1.

Hillebrand, H., Acevedo-Trejos, E., Moorthi, S.D., Ryabov, A., Striebel, M., Thomas, P.K., Schneider, M.-L., 2021. Cell size as driver and sentinel of phytoplankton community structure and functioning. Funct. Ecol. 36 (2), 276–293. http://dx.doi.org/10.1111/1365-2435.13986.

Hubbell, S.P., 2001. The Unified Neutral Theory of Biodiversity and Biogeography. Princeton University Press, Princeton, New Jersey.

Hubbell, S.P., 2005. Neutral theory in community ecology and the hypothesis of functional equivalence. Funct. Ecol. 19 (1), 166–172. http://dx.doi.org/10.1111/j.0269-8463.2005.00965.x.

Huete-Ortega, M., Cermeño, P., Calvo-Díaz, A., Marañón, E., 2012. Isometric size-scaling of metabolic rate and the size abundance distribution of phytoplankton. Proc. R. Soc. B: Biol. Sci. 279 (1734), 1815–1823. http://dx.doi.org/10.1098/rspb.2011.2257.

Huete-Ortega, M., Rodríguez-Ramos, T., López-Sandoval, D.C., Cermeño, P., Blanco, J.M., Palomino, R.L., Rodríguez, J., Marañón, E., 2014. Distinct patterns in the size-scaling of abundance and metabolism in coastal and open-ocean phytoplankton communities. MEPS 515, 61–71. http://dx.doi.org/10.3354/meps11007.

Hulburt, E.M., 1990. Description of phytoplankton and nutrient in spring in the western north atlantic. J. Plankton Res. 12 (1), 1–28. http://dx.doi.org/10.1093/plankt/12.1.1.

Hutchinson, G.E., 1957. Concluding remarks. Cold Spring Harb. Symp. Quant. Biol. 22 (2), 415–427. http://dx.doi.org/10.1101/sqb.1957.022.01.039.

Hutchinson, G.E., 1961. The paradox of the plankton. Amer. Nat. 95 (882), 137–145.

Irwin, A., Finkel, Z., Muller-Karger, F., Troccoli-Ghinaglia, L., 2015. Phytoplankton adapt to changing ocean environments. Proc. Natl. Acad. Sci. USA 112 (8), 5762–5766.

Irwin, A.J., Nelles, A.M., Finkel, Z.V., 2012. Phytoplankton niches estimated from field data. Limnol. Oceanogr. 57 (3), 787–797. http://dx.doi.org/10.4319/lo.2012.57.3.0787.

Jost, L., 2006. Entropy and diversity. Oikos 113 (2), 363–375. http://dx.doi.org/10.1111/j.2006.0030-1299.14714.x.

Kaufman, L., Rousseeuw, P.J., 1990. Finding Groups in Data: An Introduction to Cluster Analysis. In: Wiley Series in Probability and Statistics, John Wiley & Sons, http://dx.doi.org/10.1002/9780470316801.

Kiehl, J.T., Trenberth, K.E., 1997. Earth's annual global mean energy budget. Bull. Am. Meteorol. Soc. 78 (2), 197–208.

Kiorboe, T., 1993. Turbulence, phytoplankton cell size, and the structure of pelagic food webs. 29, 1–72. http://dx.doi.org/10.1016/S0065-2881(08)60129-7.

Krabberod, A.K., Deutschmann, I.M., Bjorbaekmo, M.F.M., Balague, V., Giner, C.R., Ferrera, I., Garcés, E., Massana, R., Gasol, J.M., Logares, R., 2022. Long-term patterns of an interconnected core marine microbiota. Environ. Microbiome 17 (22), http://dx.doi.org/10.1186/s40793-022-00417-1.

Latasa, M., 2007. Improving estimations of phytoplankton class abundances using chemtax. MEPS 329, 13–21. http://dx.doi.org/10.3354/meps329013.

Latasa, M., Rodriguez, F., Agusti, S., Estrada, M., 2023. Distribution patterns of phytoplankton groups along isoirradiance layers in oligotrophic tropical and subtropical oceans. Prog. Oceanogr..

Latasa, M., Scharek, R., Morán, X.A.G., Gutiérrez-Rodríguez, A., Emelianov, M., Salat, J., Vidal, M., Estrada, M., 2022. Dynamics of phytoplankton groups in three contrasting situations of the open nw mediterranean sea revealed by pigment, microscopy, and flow cytometry analyses. Prog. Oceanogr. 201, http://dx.doi.org/10.1016/j.pocean.2021.102737.

Latasa, M., Scharek, R., Vidal, M., Vila-Reixach, G., Gutierrez-Rodriguez, A., Emelianov, M., Gasol, J.M., 2010. Preferences of phytoplankton groups for waters of different trophic status in the northwestern mediterranean sea. MEPS 407, 27–42. http://dx.doi.org/10.3354/meps08559.

Lefevre, M., Vezina, A., Levasseur, M., Dacey, J.W.H., 2002. A model of dimethylsulfide dynamics for the subtropical north atlantic. Deep Sea Res. I 49, 2221–2239.

Legendre, L., Fevre, J.L., 1995. Microbial food webs and the export of biogenic carbon in oceans. Aquat. Microb. Ecol. 9, 69–77.

Legendre, P., Legendre, L., 1998. Numerical Ecology, Vol. 24. Elsevier Science BV, Amsterdam.

Litchman, E., Klausmeier, C.A., 2008. Trait-based community ecology of phytoplankton. Annu. Rev. Ecol. Syst. 39, 615–639.

Loreau, M., de Mazancourt, C., 2013. Biodiversity and ecosystem stability: a synthesis of underlying mechanisms. Ecol. Lett. 16, 106–115. http://dx.doi.org/10.1111/ele.12073.

MacArthur, R.H., 1965. Patterns of species diversity. Biol. Rev. 40, 510–533. http://dx.doi.org/10.1111/j.1469-185x.1965.tb00815.x.

MacArthur, R., 1968. The theory of the niche. In: Population Biology and Evolution. Syracuse University Press, Syracuse, N.Y..

Malerba, M.E., Palacios, M.M., Delgado, Y.M.P., Beardall, J., Marshall, D.J., 2018. Cell size, photosynthesis and the package effect: an artificial selection approach. New Phytol. 219, 449–461. http://dx.doi.org/10.1111/nph.15163.

Malone, T.C., Pike, S.E., Conley, J.D.J., 1993. Transient variations in phytoplankton productivity at the jgofs bermuda time series station. Deep-Sea Res. 40, 003–924.

Marañón, E., 2015. Cell size as a key determinant of phytoplankton metabolism and community structure. Annu. Rev. Mar. Sci. 7 (1), 241–264. http://dx.doi.org/10.1146/annurev-marine-010814-015955.

Marañón, E., Cermeño, P., Huete-Ortega, M., López-Sandoval, D.C., Mouriño-Carballido, B., Rodríguez-Ramos, T., 2014. Resource supply overrides temperature as a controlling factor of marine phytoplankton growth. PLoS ONE 9 (6), http://dx.doi.org/10.1371/journal.pone.0099312.

Margalef, R., 1974. Ecologia. Omega, Cassanova, Barcelona, p. 220.

Martin, A.P., Pondaven, P., 2006. New primary production and nitrification in the western subtropical north atlantic: A modeling study. Glob. Biogeochem. Cycles 20 (4), http://dx.doi.org/10.1029/2005GB002608.

Marty, J.-C., Chiavérini, J., 2002. Seasonal and interannual variations in phytoplankton production at dyfamed time-series station, northwestern mediterranean sea. Deep Sea Res. II 49 (11), 2017–2030. http://dx.doi.org/10.1016/S0967-0645(02)00025-5.

Marty, J.-C., Garcia, N., Raimbault, P., 2008. Phytoplankton dynamics and primary production under late summer conditions in the nw mediterranean sea. Deep Sea Res. I 55 (9), 1131–1149. http://dx.doi.org/10.1016/j.dsr.2008.05.001.

Masuda, Y., Y, Y., S, S.L., et al., 2021. Photoacclimation by phytoplankton determines the distribution of global subsurface chlorophyll maxima in the ocean. Commun. Earth Environ. 2 (128), http://dx.doi.org/10.1038/s43247-021-00201-y.

Mcnair, H., Hammond, C.N., Menden-Deuer, S., 2021. Phytoplankton carbon and nitrogen biomass estimates are robust to volume measurement method and growth environment. J. Plankton Res. 43 (2), 103–112. http://dx.doi.org/10.1093/plankt/fbab014.

Menden-Deuer, S., Lessard, E.J., 2000. Carbon to volume relationships for dinoflagellates, diatoms, and other protist plankton. Limnol. Oceanogr. 45 (3), 569–579.

Montagnes, D.J.S., Franklin, D.J., 2001. Effect of temperature on diatom volume, growth rate, and carbon and nitrogen content: Reconsidering some paradigms. Limnol. Oceanogr. 46 (8), 2008–2018. http://dx.doi.org/10.4319/lo.2001.46.8.2008.

Nekola, J.C., White, P.S., 1999. The distance decay of similarity in biogeography and ecology. J. Biogeogr. 26 (4), 867–878. http://dx.doi.org/10.1046/j.1365-2699.1999.00305.x.

Nunes, S., Latasa, M., Gasol, J.M., Estrada, M., 2018. Seasonal and interannual variability of phytoplankton community structure in a Mediterranean coastal site. Mar. Ecol. Prog. Ser. 592, 57–75.

Otero-Ferrer, J.L., 2020. Control of the Structure of Marine Picoplankton Communities by Turbulence and Nutrient Supply Dynamics (Ph.D. thesis). University of Vigo.

Pedros-Alio, C., 2012. The rare bacterial biosphere. Annu. Rev. Mar. Sci. 4 (1), 449–466. http://dx.doi.org/10.1146/annurev-marine-120710-100948, pMID: 22457983.

Racault, M.-F., Platt, T., Sathyendranath, S., Agirbas, E., Vicente, V.M., Brewin, R., 2014. Plankton indicators and ocean observing systems: support to the marine ecosystem state assessment. J. Plankton Res. 36 (3), 621–629. http://dx.doi.org/10.1093/plankt/fbu016.

Raven, J., 1998. The twelfth tansley lecture. small is beautiful: the picophytoplankton. Funct. Ecol. 12 (4), 503–513.

Ribera-D'alcala, M., Conversano, F., Corato, F., Licandro, P., Mangoni, O., Marino, D., Mazzocchi, M., Modigh, M., Montresor, M., Nardella, M., Saggiomo, V., Sarno, D., Zingone, A., 2004. Seasonal patterns in plankton communities in a pluriannual time series at a coastal Mediterranean site (Gulf of Naples): an attempt to discern recurrences and trends. Sci. Mar. 68 (1).

Righetti, D., Vogt, M., Gruber, N., Psomas, A., Zimmermann, N.E., 2019. Global pattern of phytoplankton diversity driven by temperature and environmental variability. 5 (5). http://dx.doi.org/10.1126/sciadv.aau6253.

Segura-Noguera, M., Blasco, D., Fortuno, J.M., 2012. An improved energy-dispersive x–ray microanalysis method for analyzing simultaneously carbon, nitrogen, oxygen, phosphorus, sulfur, and other cation and anion concentrations in single natural marine microplankton cells. Limnol. Oceanogr.: Methods 10, 666–680. http://dx.doi.org/10.4319/lom.2012.10.666.

Sigman, D.M., Hain, M.P., 2012. The biological productivity of the ocean. Nat. Educ. Knowl. 3 (10), URL https://www.nature.com/scitable/knowledge/library/the-biological-productivity-of-the-ocean-70631104/.

Simó, R., Vila-Costa, M., Alonso-Sáez, L., Cardelús, C., Guadayol, O., E, E.V.-D., Gasol, J.M., 2009. Annual dmsp contribution to s and c fluxes through phytoplankton and bacterioplankton in a nw mediterranean coastal site. Aquat. Microb. Ecol. 57, 43–55. http://dx.doi.org/10.3354/ame01325.

Siokou-Frangou, I., Christaki, U., Mazzocchi, M.G., Montresor, M., Ribera d'Alcalá, M., Vaqué, D., Zingone, A., 2010. Plankton in the open mediterranean sea: a review. Biogeosciences 7 (5), 1543–1586. http://dx.doi.org/10.5194/bg-7-1543-2010.

Smith, S.L., Vallina, S.M., Merico, A., 2016. Functional diversity mediates an emergent trade-off in the response of phytoplankton communities to rare versus frequent disturbances. Sci. Rep. 6 (34170), http://dx.doi.org/10.1038/srep34170.

Sommaruga, R., Hofer, J.S., Alonso-Sáez, L., Gasol, J.M., 2005. Differential sunlight sensitivity of picophytoplankton from surface mediterranean coastal waters. Appl. Environ. Microbiol. 71 (4), 2154–2157. http://dx.doi.org/10.1128/AEM.71.4.2154-2157.2005.

Steeman-Nielsen, E., 1952. The use of radioactive carbon for measuring organic production in the sea. J. Cons. Int. Explor. Mer.

Strickland, J.D.H., Parsons, T.R., 1972. A Practical Handbook of Seawater Analysis. Fisheries Research Board of Canada, Ottawa.

Stull, R.B., 2000. Meteorology for Scientists and Engineers. chapter 2: Radiation.

Tilman, D., Reich, P.B., Knops, J.M.H., 2006. Biodiversity and ecosystem stability in a decade-long grassland experiment. Nature 441, 629–632. http://dx.doi.org/10.1038/nature04742.

Tilman, D., Reich, P.B., Knops, J., Wedin, D., Mielke, T., Lehman, C., 2001. Diversity and productivity in a long-term grassland experiment. 294 (5543), 843–845. http://dx.doi.org/10.1126/science.1060391.

Unrein, F., Massana, R., Alonso-Sáez, L., Gasol, J.M., 2007. Significant year-round effect of small mixotrophic flagellates on bacterioplankton in an oligotrophic coastal system. Limnol. Oceanogr. 52 (1), 456–469. http://dx.doi.org/10.4319/lo.2007.52.1.0456.

Utermöhl, H., 1958. Methods of collecting plankton for various purposes are discussed. SIL Commun. 1953-1996 9 (1), 1–38. http://dx.doi.org/10.1080/05384680.1958.11904091.

Vallina, S.M., 2008a. Reply to comment by s. h. larsen on analysis of a potential 'solar radiation dose–dimethylsulfide–cloud condensation nuclei' link from globally mapped seasonal correlations. Glob. Biogeochem. Cycles 22, 1–5. http://dx.doi.org/10.1029/2007GB003099, 2008.

Vallina, S., 2008b. Reply to comment by Stuart H. Larsen on Analysis of a potential solar radiation dose–dimethylsulfide–cloud condensation nuclei link from globally mapped seasonal correlations. Glob. Biogeochem. Cycles (3), 3.

Vallina, S.M., Cermeño, P., Dutkiewicz, S., Loreau, M., Montoya, J.M., 2017. Phytoplankton functional diversity increases ecosystem productivity and stability. Ecol. Model. 361, 184–196. http://dx.doi.org/10.1016/j.ecolmodel.2017.06.020.

Vallina, S.M., Follows, M.J., Dutkiewicz, S., Montoya, J.M., Cermeño, P., Loreau, M., 2014a. Global relationship between phytoplankton diversity and productivity in the ocean. Nature Commun. 5, 4299.

Vallina, S.M., Le Quéré, C., 2008. Preferential uptake of ammonium over nitrate in marine ecosystem models: a simple and more consistent parameterization. Ecol. Model. 218, 393–397. http://dx.doi.org/10.1016/j.ecolmodel.2008.06.03.

Vallina, S.M., Martinez-Garcia, R., Smith, S.L., Bonachela, J.A., 2019. Models in microbial ecology. In: Schmidt, T.M. (Ed.), Encyclopedia of Microbiology (Fourth Edition), fourth ed. Academic Press, Oxford, pp. 211–246. http://dx.doi.org/10.1016/B978-0-12-809633-8.20789-9.

Vallina, S.M., Word, B.A., Dutkiewicz, S., Follows, M.J., 2014b. Maximal feeding with active prey-switching: A kill-the-winner functional response and its effect on global diversity and biogeography. Prog. Oceanogr. 120, 93–109. http://dx.doi.org/10.1016/j.pocean.2013.08.001.

van den Engh, G.J., Doggett, J.K., Thompson, A.W., Doblin, M.A., Gimpel, C.N.G., Karl, D.M., 2017. Dynamics of prochlorococcus and synechococcus at station aloha revealed through flow cytometry and high-resolution vertical sampling. Front. Mar. Sci. 4, http://dx.doi.org/10.3389/fmars.2017.00359.

Verity, P.G., Robertson, C.Y., Tronzo, C.R., Andrews, M.G., Nelson, J.R., Sieracki, M.E., 1992. Relationships between cell volume and the carbon and nitrogen content of marine photosynthetic nanoplankton. Limnol. Oceanogr. 37 (7), 1434–1446. http://dx.doi.org/10.4319/lo.1992.37.7.1434.

Villarino, E., Watson, J.R., Jonsson, B., Gasol, J.M., Salazar, G., Acinas, S. G., Estrada, M., Massana, R., Logares, R., Giner, C.R., Pernice, M.C., Olivar, M.P., Citores, L., Corell, J., Rodriguez-Ezpeleta, N., Acuña, J.L., Molina-Ramirez, A., Gonzalez-Gordillo, J.I., Cozar, A., Marti, E., Cuesta, J.A., Agusti, S., Fraile-Nuez, E., Duarte, C.M., Irigoien, X., Chust, G., 2018. Nature Commun. 9 (142), http://dx.doi.org/10.1038/s41467-017-02535-8.

Ward, J.H., 1963. Hierarchical grouping to optimize an objective function. J. Amer. Statist. Assoc. 58, 236–244.

Ward, B.A., Follows, M.J., 2016. Marine mixotrophy increases trophic transfer efficiency, mean organism size, and vertical carbon flux. Proc. Natl. Acad. Sci. 113 (11), 2958–2963. http://dx.doi.org/10.1073/pnas.1517118113.

Weistuch, C., Zhu, J., Deasy, J.O., Tannenbaum, A.R., 2022. The maximum entropy principle for compositional data. BMC Bioinformatics 23 (449), http://dx.doi.org/10.1101/2022.06.07.495074.

Westberry, T., Behrenfeld, M.J., Siegel, D.A., Boss, E., 2008. Carbon-based primary productivity modeling with vertically resolved photoacclimation. Glob. Biogeochem. Cycles 22 (2), http://dx.doi.org/10.1029/2007GB003078.

Winn, C.D., Campbell, L., Christian, J.R., Letelier, R.M., Hebel, D.V., Dore, J.E., Fujieki, L., Karl, D.M., 1995. Seasonal variability in the phytoplankton community of the north pacific subtropical gyre. Glob. Biogeochem. Cycles 9 (4), 605–620. http://dx.doi.org/10.1029/95GB02149.

Wootton, J., 2005. Field parameterization and experimental test of the neutral theory of biodiversity. Nature 433 (7023), 309–312.

Yachi, S., Loreau, M., 1999. Biodiversity and ecosystem productivity in a fluctuating environment: The insurance hypothesis. Proc. Natl. Acad. Sci. USA 96, 1463–1468.